Discover Electrochemistry

RESEARCH Open Access

Establishing a living systematic review of characterisation and parameter reporting in lithium-ion and lithium–sulfur cathode research

Liam Bird[1,2,3*], Yiheng Shao[1,2,3], Boyi Pang[3,4], James Robinson[3,4] and Paul Shearing[1,2,3]

*Correspondence:
Liam Bird
liam.bird@eng.ox.ac.uk
[1]The ZERO Institute, Holywell House, Osney Mead, Oxford OX2 0ES, UK
[2]Department of Engineering Science, University of Oxford, Parks Road, Oxford OX1 3PJ, UK
[3]The Faraday Institution, Quad One, Becquerel Avenue, Harwell Science and Innovation Campus, Didcot OX11 0RA, UK
[4]Advanced Propulsion Lab (APL), Marshgate, London E20 2AE, UK

Abstract

Advancing energy storage and decarbonising transportation while improving today's Lithium-ion technology remain crucial, however it is equally important to pioneer new battery systems, such as lithium–sulfur (Li–S), which can meet future demands. Despite decades of progress in materials synthesis and characterisation, inconsistencies in parameter reporting and testing standards continue to limit reproducibility and cross-comparison across the battery literature. Here, we present a systematic meta-analysis of nickel–manganese–cobalt oxide (NMC) Li-ion and Li–S cathode systems, using a Python-based graphical user interface to standardise data extraction for electrode fabrication, electrochemical testing, and physical characterisation. The analysis reveals that even for the higher-technology readiness level (TRL) NMC chemistry, key experimental parameters such as electrode thickness, testing temperature, and formation protocols are frequently omitted. Both battery systems also exhibit inconsistencies in analytical procedures and ambiguity in the understanding of underlying principles when interpreting characterisation results. Our findings highlight systematic under-reporting of scalable manufacturing parameters and essential comparability metrics across both chemistries. This work establishes a cross-chemistry benchmark for transparent and reproducible reporting, providing a foundation for accelerating the translation of materials-level advances toward higher TRLs.

1 Introduction

Increasing global demand for electrified transport, including electric vehicles (EVs), and distributed electricity generation has prompted research interest in rechargeable batteries. This includes intercalation-based lithium-metal oxide chemistries (Li_xCoO_2, LCO, and $Li_xNi_yMn_zCo_{(1-y-z)}O_2$, NMC) which are established in consumer electronics and personal EVs. However, developments in lightweight batteries such as conversion chemistry-based lithium–sulfur (Li–S) are required to enable weight-critical applications including aerospace and road-freight transport [1].

Battery research articles typically focus on a specific component (i.e. anode, cathode, or electrolyte), however interactions within the cell system mean that the effect of each component cannot be assessed in isolation, even in a half-cell configuration where one electrode is replaced by lithium metal. Journals including ACS [2], Batteries Europe [3], Joule [4], the Journal of Power Sources [5], and Wiley [6] have published guidelines for key metrics to include in articles reporting developments in electrode formulations to ensure transparency in comparing electrochemical performance. These guidelines are voluntary, and previous meta-analyses of Li–S literature [7–9] found inconsistency in which of these metrics are reported. Additionally, a variety of physical, chemical, and electrochemical characterisation methods are used to measure the properties of electrode materials, however different journal articles report different combinations of characterisation techniques [10] applied to different measurands (for example, electrode materials vs. electrodes containing binder and additives).

Given its widespread commercial adoption with gigafactory-scale fabrication facilities [11], NMC has a high technology readiness level (TRL) assessed at 9 on NASA's definition scale [12]. Meanwhile, Li–S is approaching commercial-scale manufacture, with prototypes and demonstrators available, but no mass-market adoption at time of writing, placing Li–S at a TRL of 5–6 [13]. Their distinct operating regimes make it likely that Li–S and NMC batteries will play complementary, rather than directly competitive, roles in electrification [1], and the unique technical challenges posed by each chemistry will necessitate different innovation trajectories to reach a similar TRL. Acknowledging these differences, this meta-analysis investigates whether the degree of standardisation in Li–S research is comparable to NMC, and seeks to identify whether lessons from the higher TRL NMC can be applied to advance Li–S development.

This meta-analysis investigates the frequency with which different recommended metrics, and which combinations of characterisation methods, are reported for battery chemistries with different TRLs. Data corresponding to the metrics recommended in journal guidelines (summarised in Table S1) from 200 articles were collated. With a view to consistent comparison, this analysis focuses on published work primarily focused on the electrochemically active material in the cathode (i.e. positive electrode) for both Li–S and Li-ion cells, referred to as CAM. In Li–S cells, this includes the conductive material used to form a composite with the sulfur (typically carbon), and in Li-ion cells this refers to the NMC. Section 2 presents a short overview of the current status of each battery chemistry, highlighting turning points in the development of each. Section 3 covers the methodology for collating the data from the 100 Li–S and 100 NMC-focussed articles, and defines key categories and nomenclature used in the later analysis. The collated data is analysed with a focus on electrode synthesis (Sect. 4), electrochemical testing (Sect. 5), and physical characterisation (Sect. 6). Throughout these analysis sections, the macro-scale trends identified are supported by ∼3 representative examples drawn from the articles included in the meta-analysis: these example lists are not exhaustive, but intended to indicate the order of magnitude of parameter values, typical combinations of components, or frequently-sought characterisation outcomes. The complete dataset including further examples is available in the Supplementary Information. Finally, Sect. 7 presents a discussion and outlook of the extent to which currently-available data is useful in reproducible battery research, and identifies opportunities for improvement in future publications.

2 Status of Li-ion and Li–S technology

NMC is currently the dominant Li-ion battery chemistry for light-duty EVs, including cars, accounting for ∼ 60% of EV battery sales in 2022 [14] and projected to continue to dominate the market alongside lithium iron phosphate (LFP) to 2050 [11, 14]. The combination of Ni, Mn and Co results in improved thermal stability compared to Li_xCoO_2, reduced degradation compared to the effects of cation mixing in Li_xNiO_2, and improved gravimetric capacity compared to $Li_{0.5}Mn_2O_4$ [15–18]. Following initial developments in the use of layered transition metal oxides and spinels in Li-ion cathodes from 1980 onwards [19–22], and specifically NMC 111 from 1999 onwards [23, 24], research focus and commercialisation have shifted towards nickel-rich chemistries [11] including NMC 532 [25], 622 [26], 811 [27, 28], and 955 (i.e. $LiNi_9Mn_{0.5}Co_{0.5}$ [29]. The motivations for decreasing Co content include human rights and environmental concerns [30] and geopolitical sensitivity associated with Co mining, and the aim of developing Ni-rich chemistries is therefore to ensure supply chain security and minimise cost. Additional current research focuses include mitigating capacity degradation, including the use of single-crystal NMC [31] to mitigate cracking, and by stabilising the interface between the active material and electrolyte by using coatings [16] or core-shell structures with a Ni-rich core and increasing Mn concentration towards the surface [17]. Other approaches seen in this meta-analysis include low concentrations of dopants including Mg (e.g. [32–34]), Al (e.g. [2, 35, 36]) and Mo (e.g. [2, 37]), with the aim of stabilising the layered transition metal oxide structure during (de-)intercalation of Li^+.

Meanwhile, Li–S batteries are currently moving from laboratory scale demonstrators [13] to pilot-line scale production (e.g. [38–41]), predominantly targetting applications in small-scale air transport. By contrast to the intercalation mechanism in conventional Li-ion electrodes, Li–S cells use the reversible chemical conversion of solid sulfur (S_8) to solid lithium sulfide (Li_2S) *via* a series of soluble lithium polysulfides (LiPS). Although this gives Li–S cells a higher theoretical gravimetric capacity of 1675 mAh g^{-1}, compared to ∼277 mAh g^{-1} for NMC, the diffusion of the soluble LiPS into electrical isolation from the cathodic matrix results in capacity degradation, a key challenge to their widespread adoption. To address this issue, research initially focussed on tuning electrolyte solubility to mitigate diffusion [42, 43], however renewed interest in Li–S research was catalysed by Ref [44]'s demonstration of an optimised conductive cathodic matrix, consisting of a templated hierarchically porous carbon. Optimising the morphology of the cathodic matrix to prevent LiPS diffusion remains a key focus of Li–S research [10], alongside incorporation of functional groups and dopants [45–47]. Ongoing challenges to the widespread adoption of Li–S batteries include incompatibility of the widely-used electrolyte additive $LiNO_3$ with UN Transport Recommendations [48], and the offsetting of the high theoretical gravimetric capacity due to excess electrolyte utilisation [10, 49]. Approaches to this include going foregoing the solid–liquid-solid phase transformation by tuning the interaction between the host matrix and the electrolyte [50], however this meta analysis reflects the existing focus on host matrix morphology and ether-based electrolytes.

3 Methodology

Data corresponding to recommended parameters collated from 5 voluntary reporting checklists, summarised in Table S1, were collected using a graphical user interface (GUI) implemented in a Python Jupyter notebook (available in Supplementary Information) to facilitate fast, standardised data entry for a large number of parameters, including pre-filled entries for the most common values. The GUI also includes a checkbox grid for characterisation techniques and corresponding measurands, grouped by data type and measurement probe, specifically: morphological (mainly qualitative, optical or electron imaging), structural (mainly X-ray derived), vibrational spectroscopy, pore size and surface area, and electrode composition. The measurands were classified as: the uncycled electrode (including the active material and, where present, the conductive carbon and binder coated on a metal current collector), *in-situ* or *operando* characterisation undertaken during electrochemical testing, and *post-mortem* characterisation of electrodes recovered from cycled cells. Additional measurands are the 'raw materials', which corresponds to the NMC powder in NMC-related articles, and generally refers to the conductive host matrix in the absence of sulfur in Li–S articles, while 'composite' is used specifically for the S/C composite in Li–S articles to differentiate this from the conductive host.

Parameter information was collated from a total of 200 articles (100 Li–S and 100 NMC articles), with data drawn from both the main text and supplementary information. Articles were identified using the Web of Science database and through citations in relevant review articles, with the most recent search performed on 17/08/2025. To be eligible for inclusion, articles were required to report the galvanostatic cycling capacity corresponding to a cathode under investigation, where the target of the investigation may be the method of synthesising the active material (e.g. S/C composite, NMC) or electrode manufacturing method (e.g. modifying quantity of conductive additive). For database searches, the following search combinations were used. Terms related to 'electrolyte', 'separator', 'anode', and life-cycle assessment and resource recovery were excluded from article titles to return articles whose central focus is on cathode materials development.

Li–S: "lithium–sulfur" OR"Li–S" OR "lithium-sulphur" OR "lithium sulfur" or"lithium sulphur" OR "Li S" (Topic) and cathode (All Fields) not electrolyte OR separator OR interlayer OR coating OR anode (Title) not "all-solid-state" OR "solid state" OR "solid electrolyte" (Title) not Review (Document Type)

NMC: nickel AND manganese AND cobalt AND battery (All Fields) or NMC OR NCM AND battery (All Fields) not NMC OR NCM (Author) not algorithm OR regression OR "life cycle analysis" OR "life cycle assessment" OR recovery OR sodium OR potassium (All Fields) not recycling OR "solid state" OR "battery management system" OR electrolyte (Title) not Review (Document Type)

4 Electrode preparation

4.1 Electrode slurry and coating

The electrode composition, including the ratio of CAM, binder, and conductive carbon additive (where used) is fundamental to reproducibility of reported results and to direct comparison of electrochemical results, especially for novel CAM. The content of these electrode constituents was reported by 96 % of articles included in this meta analysis

(the data is omitted in [51–53], and values are included in a previous referenced publication by one [36]), and is typically reported as relative contents of each constituent, e.g. 80: 10: 10 by weight CAM: binder: conductive additive. Assuming that the electrode slurry is homogeneous, in principle these ratios are relevant to all scales of manufacture. However, the electrode homogeneity is also affected by factors including the electrode mixing, coating, and drying processes, which may in turn be determined by the scale of electrode synthesis. For example, ∼10 s-100 s mg quantities of novel materials prepared in a laboratory are likely to be prepared using manual mixing or small planetary mixers, while optimising the mixing procedure using pilot-line scale equipment was shown to strongly affect the electrochemical behaviour of electrodes produced in ∼100 s mL batches [13, 54]. Consequently, the ACS [2] and JPS [5] voluntary checklists include the scale of electrode synthesis, however as shown in 1a, this is reported by 64 and 21 Li–S and NMC related articles respectively. The absolute quantities of electrode precursors are most commonly reported (45 Li–S articles, 10 NMC articles). For example, Ref [33] specifies the use of 2.079 g nickel nitrate and 5.072 g manganese nitrate (*inter alia*) when synthesising NMC, and Ref [55] reports the use of 1.2 g V_2O_5 and 2.5 g oxalic acid as precursors to forming hollow spheres which were used as a host matrix for Li–S cathodes. In the latter, although the absolute quantity of sulfur is not specified (the relative quantity, 80 wt%, is measured empirically), these precursor values are indicative of the total volume of electrode slurry and associated mixing conditions.

Where electrodes are coated on metal current collectors (rather than freestanding), the electrode structure is also affected by the electrode slurry viscosity during coating and mixing [56]. However, the solid content of the electrode slurry is reported by only 8 % articles, including Refs [54] and [57] where the electrode slurry solvent was the subject of optimisation. Furthermore, Ref [57] demonstrates the significant effect of binder processing history on the electrochemical behaviour of Li–S electrodes, while Ref [58] investigates the effect of slurry solvent on the dispersion of electrode powder and consequent electrode structure. However few articles explicitly report the method of binder preparation, including the pre-dissolution of binder in solvent before mixing with the other dry components [20, 34, 57–59]. Refs [60, 61] specify the use of pre-dissolved binders (LA133 and polyvinylidene fluoride, PVDF), with Ref [61] specifying its viscosity. In other articles, the amount of solvent used is unspecified, in some cases referred to as “an appropriate amount" [62], or “enough" [63], indicating experimental experience in

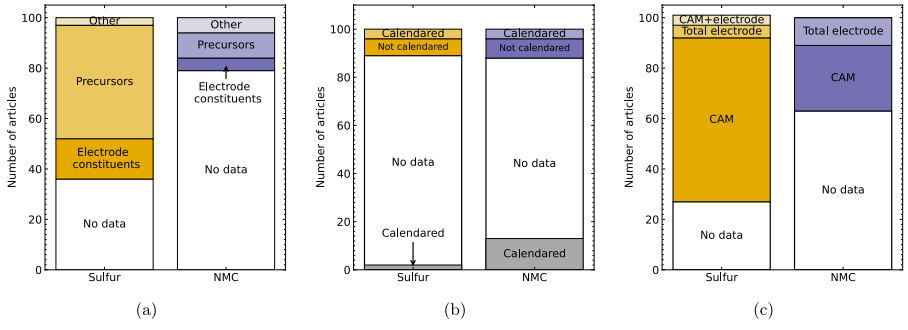

Fig. 1 Frequency of reporting electrode synthesis parameters for Li–S and NMC articles. **a** Production scale, e.g. ∼ mg - ∼g scale: Electrode constituents refers to materials used directly in cell, e.g. sulfur, NMC powder, and precursors refers to e.g. glucose used for carbonisation, NMC hydroxides. **b** Electrode thickness and calendering, where grey bars at bottom show reports of calendering without reporting the thickness. **c** Areal loading of cathode active material (CAM), total electrode including binder and additives, or reporting both CAM and total electrode values

producing a slurry with suitable viscosity. The energy demand for electrode drying contributes approximately 12–13 % to the embodied energy of cell manufacture [54, 64, 65], and the replacement of NMP with non-toxic alternatives compatible with binders free from per- and polyfluoro alkyl substances (PFAS) is a research priority for both sustainable initial manufacturing and electrode recycling [66, 67]. Therefore, while the goal of adjusting the electrode slurry viscosity is to produce a homogenous electrode with a uniform thickness and/ or areal loading (discussed below) after removal of the solvent, the slurry solvent content and associated electrode drying conditions are useful parameters for reproducibility at the lab scale and are relevant for scale-up.

4.2 Electrode thickness and calendering

The electrode thickness, porosity, and associated areal loading of CAM influence the cell-level gravimetric (Wh kg^{-1}) and volumetric (Wh L^{-1}) energy density. The ratio of both the mass and volume of CAM to auxiliary cell components, including the metallic current collector and the polymer separator, can be increased both by using thicker electrodes to achieve a higher areal loading of CAM (kg m^{-2}) and by increasing their volume density by calendering (compression with a defined load and temperature). In principle, the electrode thickness is a readily accessible measurand, however practical difficulties in measuring it are reflected by its reporting in 11 and 12 of Li–S and NMC articles respectively (see Fig. 1b). As previously noted in Ref [7], the areal loading of active material is reported more frequently (73 % of Li–S, 37 % of NMC articles), potentially because of its accessibility *via* electrode mass. Where the electrochemical performance is reported for multiple different areal loadings of electrodes with the same composition (e.g. NMC [68], Li–S [55, 57, 58, 69–76]), the effect of electrode thickness can be qualitatively inferred based on the correlation between greater thickness and higher areal mass loading.

In some instances, the thickness was indicated *via* the coating setting, typically Doctor blade height (Li–S [77], NMC [22, 61, 78–81]), although providing an indicative value, the realised thickness after solvent evaporation depends on factors including the solid content of the slurry (discussed above). In other instances, the electrode thickness was specified based on the known dimensions of a template or precursor, for example those used for freestanding electrodes for Li–S cells [82, 83], or measured directly using a micrometer or SEM (Li–S [84–86], NMC [59, 87]). However, increasing the thickness of Li–S cathodes may limit their rate capability and reversible capacity utilisation due to longer diffusion distances for Li^+ ions perpendicular to the cathode/ separator interface [88]. Furthermore, additional flocculent carbon black per unit area introduces more surface area requiring contact by the electrolyte: Ref [60] calculated that, due to the higher carbon black content of Li–S vs. Li-ion electrodes, their porosity may be as high as 70% compared to c. 30% [89] for Li-ion cathodes. Percolating this pore network requires additional electrolyte, potentially offsetting beneficial weight savings from reduced areal requirement for auxiliary components. On one hand, porosity and concomitant electrolyte requirement, in addition to the electronic conductivity (due to contact between electrode particles), can be controlled via calendering. For example, Ref [60] demonstrated a linear increase in conductivity when decreasing the electrode porosity to 50% in Li–S electrodes. On the other hand, decreased porosity is accompanied by increased tortuosity of connections between pores where tortuosity is defined as the ratio of the

total path taken length though the porous material to the linear distance between the path's start and end points [90]. Precipitation of Li_2S during discharge may therefore block these pathways, decreasing the reversible capacity compared to lower tortuosity electrodes [90], which is supported by Ref [60]'s observation of lower wettability and lower pore visibility in calendered vs. uncalendered electrodes. 1 article included in this meta-analysis reported the electrode tortuosity quantitatively, calculated from EIS measurements of symmetrical (cathode/ cathode) coin cells [58]. The tortuosity value may also be determined from tomographic data, for example using tools such as TauFactor [91], however as shown in Sect. 6 this data is frequently unavailable to researchers, likely due to high cost and the time-consuming nature of these techniques, with X-ray computed tomography reported by 5 Li–S [57, 58, 76, 92, 93] and 1 NMC article [59], and focussed ion beam scanning electron microscopy (FIB-SEM) reported by 2 Li–S [57, 94] and 7 NMC articles [32, 95–100].

Despite the control offered by calendering over the electrode thickness, as shown by the grey bars in in Fig. 1b, 15 articles report the use of calendering without reporting the thickness. Instead, the calendering parameters are reported in terms of pressure (e.g. 3 kN [2], 10 N mm^{-1} [101]): this is consistent with the Joule voluntary reporting checklist [4], the only one to specify calendering parameters. Although one outcome of calendering is improving the uniformity of electrode thickness following coating, controlling the interaction with the electrolyte *via* porosity and tortuosity directly affects the electrochemical behaviour of the cell, therefore the results of calendering may be reported as a function of electrode porosity [60, 102]. For scale-up, further parameters including the speed and heat applied are required for reproducibility.

5 Electrochemistry

5.1 Statement of nominal capacity

Reporting galvanostatic cycling results for the electrode material under test was a prerequisite for inclusion of an article in this meta-analysis. The galvanostatic rate used was specified in terms of current (mA or mA g^{-1}), or C rate (where 1C = 1 charge/ discharge in 1 h). Despite this, and the recommendation by four of the publisher's voluntary reporting guidelines ([2, 4–6]), as shown in Fig. 1b, the gravimetric capacity used to determine the C rate or current density was specified by 49 NMC articles. By contrast, 90 Li–S articles explicitly state the theoretical capacity of sulfur, likely because its high gravimetric capacity compared to LCO is a key motivator for its development (with one article referring to sulfur's theoretical capacity as "marvellous" [73]). The less frequent reporting in NMC articles may be due to the undefined practical maximum (de)-intercalation of Li in NMC (i.e. the stoichiometry of x in $Li_xNi_yMn_zCo_{1-y-z}O_2$) for novel NMC stoichiometries, while the requirement for 16 Li^+ ions for the chemical reduction of S_8 to Li_2S is well-defined. To this end, 3 NMC article reported the use of a slow initial cycle (Sect. 5.3) to determine the practical capacity of the cell for use in setting the C rate. However, as shown in Fig. 2a, the theoretical capacity is specified with approximately equal frequency for different types of NMC, including 'other' stoichiometries than the commonly used types specified. While the theoretical capacity of $Li_xNi_yMn_zCo_{1-y-z}O_2$ can be easily calculated assuming that x=1, where there is no explicit basis for C rate calculation and the current density is unspecified, there is no self-contained means to directly compare the galvanostatic current densities between articles.

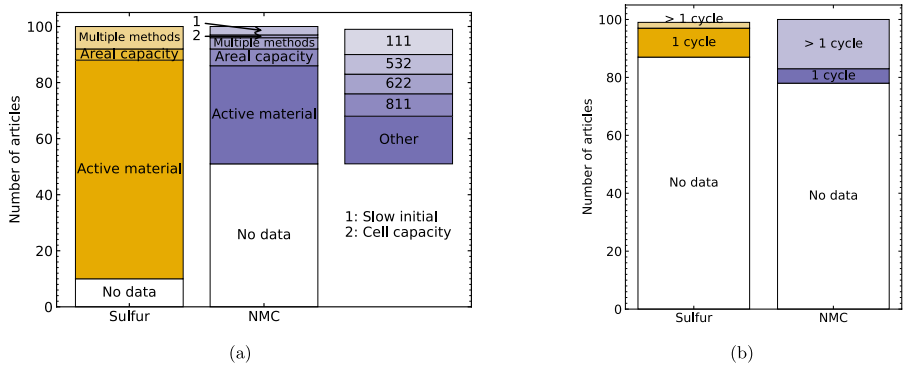

Fig. 2 Frequency of reporting parameters for gravimetric cycling. **a** Basis for calculating cell capacity or C rate, where right bar shows number of articles where assumed capacity is reported for each NMC stoichiometry. 'Active material': theoretical capacity in mAh g^{-1}, 'Areal capacity': mA cm^{-2}. **b** Use of slow formation cycle prior to long-term cycling

However, when converting reported current densities to C rates in Sect. 5.2 using an assumed theoretical capacity of 277 mAh g^{-1} for NMC, integer- or near-integer values of N for for C/N or NC were obtained, suggesting that this value is used for calculation even where not explicitly stated.

5.2 C rate ranges

The minimum (left columns) and maximum (right columns) C rates are summarised in Fig. 3, with 0.1C and 0.2C the most commonly used minimum rates used in the analysed articles. Where the galvanostatic cycling conditions were specified in terms of current density (mAh g^{-1}), these values were converted to C rate using assumed theoretical capacities of 1675 mAh g^{-1} and 277 mAh g^{-1} for Li–S and NMC articles respectively. When comparing the plots, note that 1C corresponds to ∼275 mA g^{-1} for NMC (see discussion above), and 1675 mA g^{-1} for Li–S. The C rates summarised in Fig. 3 represent a mixture of long-term cycling at a continuous rate, and step-by-step rate capability tests to reach higher values such as 10C. A breakdown of the frequency of use of different rate capability protocols for Li–S cells is available in Ref [7], however the focus of this work is comparing whether the most materials-level characterisation conditions are representative of targets for commercial cells. The US Advanced Battery Consortium (USABC) has published targets of 350 Wh/kg at cell level using C/3 (i.e. 20 min charge) for EVs in general [103], and Refs [104, 105] propose targets of 3–6 C for electric vertical take-off and landing (eVTOL) vehicles with pulse power requirement up to 12 C. However, other roadmaps (e.g. [1, 106, 107]) specify targets for power density in terms of W/kg or W/L, referring the mass or volume to the cell or pack-level, making direct comparison to C rate reporting challenging.

Furthermore, unlike the C rate, the energy and power density are functions of cell voltage. Figure 4 shows the frequency of using different upper and lower cut-off ranges used in more than 1 article for Li–S and NMC, with the vertical height spanning the voltage range specified and the width corresponding to the number of reports. The operating windows are plotted on the same y-axis to highlight the likelihood of Li–S and NMC fulfilling complementary, rather than competing, roles in applications. In Fig. 4a, a lower cut-off of 1.7 V is indicated with a horizontal line, corresponding to the voltage at which the commonly-used (73 % of Li–S articles [7]) additive $LiNO_3$ undergoes irreversible

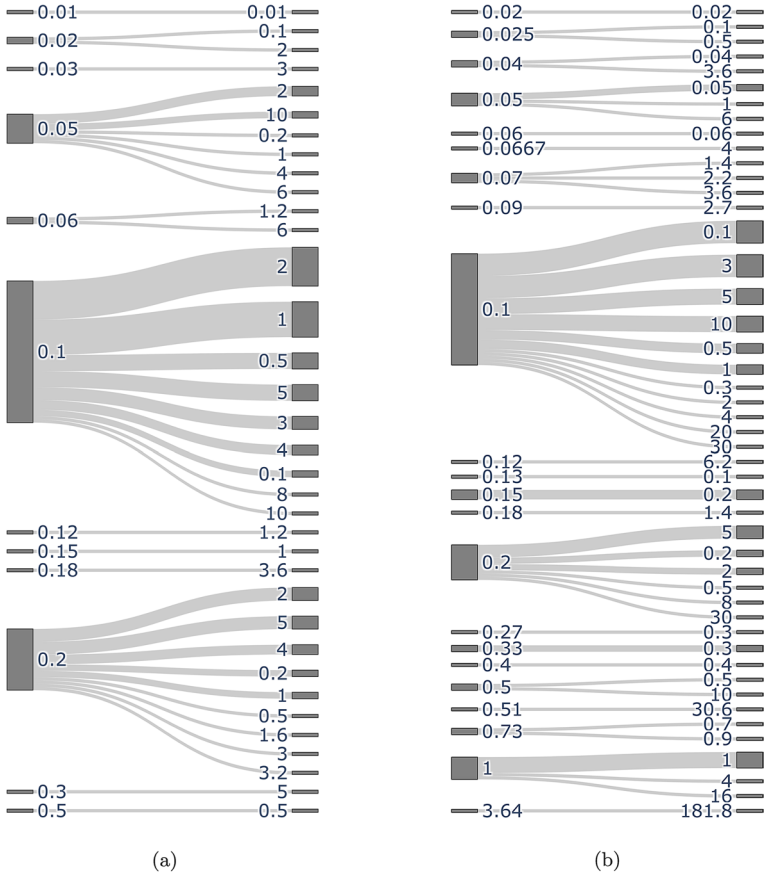

Fig. 3 Minimum and maximum C rates reported for **a** Li–S and **b** NMC articles. Left columns show minimum reported rate, right columns show maximum reported rate (for either continuous or progressive rate capability cycling). Joining line thickness proportional to number of articles reporting each combination of minimum/maximum rates

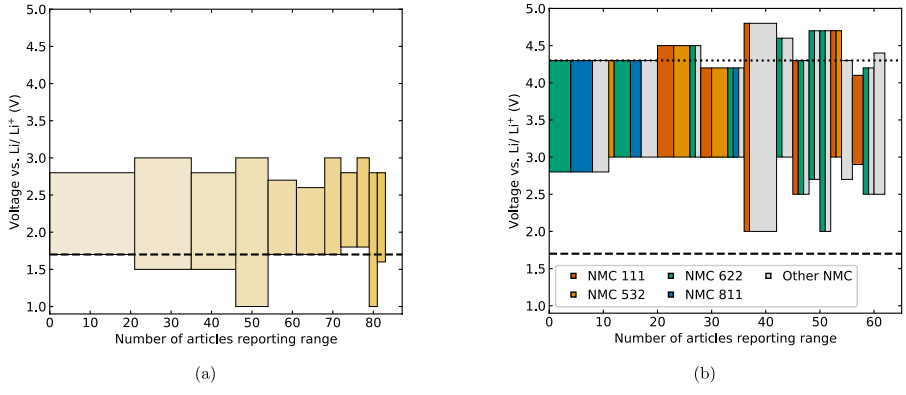

Fig. 4 Minimum and maximum voltage ranges for galvanostatic cycling reported by at least one article for **a** Li–S articles and **b** NMC articles. Dashed line in **a** at the minimum voltage where $LiNO_3$ is stable, dashed and dotted lines in **b** show window where capacity degradation is minimised in NMC full cells

decomposition [108, 109]. Similarly, Fig. 4b indicates the upper cut-off voltage at 4.3 V, corresponding to oxygen evolution from the NMC structure which contributes to an irreversible capacity loss [110]. Notably, 85 % of the NMC-related articles included in this meta-analysis are half-cells with lithium anodes, so were unaffected by processes at

the graphite anode outside of this voltage window in commercial cells [111]. The bars in Fig. 4b are further broken down by NMC stoichiometry, with 'other' including approximately equal numbers of cells with x≥ 0.8 and x<0.8 for $LiNi_xMn_yCo_{(1-x-y)}O_2$. When operating in the same conditions with upper cut-off voltage ≤ 4.15V, cells with high nickel content cathodes (x≥0.8) have higher gravimetric energy than those with lower nickel content (NMC622, NMC532, NMC111) [16], while cells with the same gravimetric capacity operated over wider voltage ranges have higher energy density. However, when charging cells with high nickel content to higher upper cut-off voltages, initial gains in charge capacity are offset by accelerated degradation [81, 112, 113], associated with processes including a phase transition at 4.1 V vs. Li/ Li^+, resulting in volume change and loss of structural integrity [113–115]. This is consistent with the data for NMC811 in Fig. 4b, where all reported high-nickel samples were charged to a maximum of 4.3V. The use of upper cut-off voltages above 4.3V for 'other' NMC compositions likely reflects the data collection process, where the maximum and minimum voltages within each article are recorded, and therefore captures articles where different voltage windows are used for non-standard NMC compositions (including high nickel) to demonstrate stability or degradation (e.g. [81, 116, 117]).

5.3 Formation cycles

The C rates shown in Fig. 3 represent the rates used for long-term cycling stability evaluation, however, Fig. 2b shows that 22 NMC articles and 7 Li–S articles additionally used slow initial cycles. This typically involved cycling at a median rate of 0.10 or 0.05 for NMC and Li–S articles respectively, with the highest number of cycles specifically used for 'formation' being 10 for NMC [116]. Where used in Li–S articles, the slow initial cycles aim to 'activate' the sulfur. While the commonly-used melt-infiltration method of S/C composite synthesis aims to form a thin layer of sulfur at the electrochemically active interface, as evidenced by XRD, crystalline α-S_8 commonly exist in these as-produced porous structures [7, 44]. Here, the sulfur in the 'core' of these ionically and electronically insulating particles initially isolated from the interface. The slow formation cycle therefore aims to enable the reduction of sulfur and subsequent oxidation of LiPS to sulfur while minimising the influence of diffusion and/ or rate limitations that may occur at higher current densities [118]. In commercial Li-ion cell manufacture, including NMC cells, an initial slow formation cycle is used to produce a stable solid-electrolyte interphase (SEI) and cathode-electrolyte interphase (CEI), which mitigate ongoing decomposition reactions between the electrolyte and electrically conductive interfaces of the electrodes [119]. The infrequency of using a formation cycle in the materials development-focussed articles included here may be attributed to the majority use of half-cells (85% in this dataset) with lithium metal anodes, rather than commercially representative full cells with lithiated graphite anodes (12% in this dataset), leading to different interphase requirements which may lead researchers to forego equivalent formation cycling to that used in full cells. However, at higher TRL, confirming the effect of the formation cycle on the engineered cathode is relevant in the context of optimising formation conditions: in commercial NMC manufacture, the formation and ageing process accounts for ∼20–25% of the total energy demand for cell manufacture [65, 119, 120], so optimising these steps is instrumental in reducing the embodied energy of cells.

5.4 Temperature

All of the reporting guidelines surveyed for this meta-analysis recommend reporting the environmental temperature used during cycling, however as shown in Fig. 5a this is reported by 23% of Li–S and 45% of NMC articles respectively. The reported temperatures were classified as 'room temperature' where this is explicitly stated but no temperature value or means of direct monitoring and control is reported, 'constant' where a temperature value is specified and is assumed to be directly monitored and/or maintained, and 'under test' where the electrochemical performance of the cells is investigated as a function of cycling temperature. The specified 'constant' temperature is typically close to room temperature (e.g. 25± 5°C). However, Ref [121] demonstrated the difference between cycling Li-ion pouch cells in temperature controlled chambers at 25°C versus ambient conditions, where self-heating in the absence of active air circulation caused the cells in ambient conditions to operate at 27°C. Although this is a small variation, on a similar scale to diurnal temperature fluctuations in a laboratory, in Li-ion full cells this affected cell longevity due to the competing effects on lithium plating and SEI formation around a pivotal temperature of 25°C in commonly-used electrolytes in Li-ion cells. While temperature ranges of ∼25–60 °Cwere reported in the NMC-focussed articles in this meta-analysis [37, 122–124] the Li–S examples included here used a wider range from ≤ - 10–50 °C[92, 125], with the low temperature testing likely motivated by the target applications of Li–S cells in aerospace environments [126]. Li–S cells show a similar trend to Li-ion, with higher temperatures corresponding to similar or higher initial capacity compared to 25 °C but more rapid capacity degradation, however this trend is caused by different physical processes in Li–S cells. The lower capacity retention at high temperatures is associated with increased overpotential, particularly affecting the lower discharge voltage plateau [92, 127], while for Li–S cells with similar electrodes and electrolytes the upper discharge plateau capacity and overpotential are less affected at lower temperatures than the lower plateau, corresponding to the slower kinetics [44] of the conversion of $Li_2S_{6,4}$ to Li_2S_2 and Li_2S compared to the initial reduction of S_8 to long-chain LiPS [128]. The role of kinetics in the temperature dependence of Li–S performance is also demonstrated by Ref [125], who demonstrated a reduced capacity loss at lower temperatures by optimising the conductive host matrix to mitigate the higher impedance at the electrolyte/ electrode interface encountered at lower temperatures. Therefore, future reporting would benefit from inclusion of the temperature

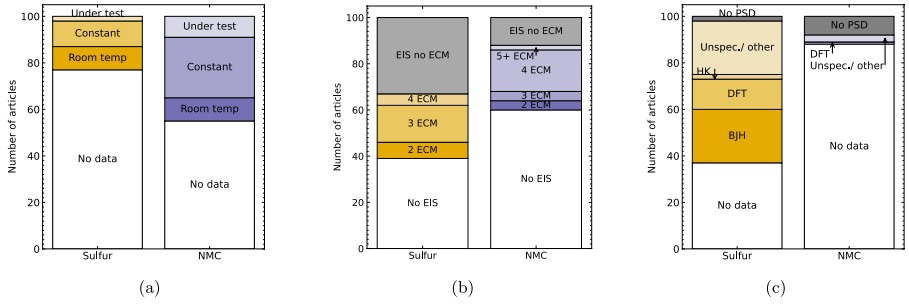

Fig. 5 Frequency of reporting electrochemical parameters. **a** Temperature during cycling ('under test': capacity investigated as a function of temperature), **b** Electrochemical impedance spectroscopy (EIS) and number of components in series in equivalent circuit model (ECM), **c** N_2 adsorption results for BET (all coloured bars) and method of pore size distribution determination (HK: Horwath Kazoe, DFT: Density functional theory, BJH: Barret-Joyner-Halenda, 'other' includes mercury intrusion porosimetry)

of the lab during electrochemical cycling, including the range of ambient temperatures where this is not directly controlled, to enable valid comparison between studies.

5.5 Electrolyte

Figure 6a shows the frequency with which the electrolyte content of prototype cells is reported in articles included in this meta-analysis. The high theoretical gravimetric capacity of Li–S cells, based on the mass of the active material S_8, can be offset by the relatively large contribution to the cell-level mass from the liquid electrolyte, leading to the identification of target electrolyte/ sulfur (E/S) ratios to ensure that Li–S cells have competitive gravimetric energy density at the cell level. These targets are typically specified in μL electrolyte per mg S_8, including 5 μL mg^{-1} [49], 3 μL mg^{-1} [13], or 2 μL mg^{-1} in a pouch cell [10]. The use of excess electrolyte in Li–S cells minimises the influence of capacity degradation processes associated with higher electrolyte viscosity, preventing percolation of the microporous structure, where the concentration of dissolved S_8 and LiPS is higher [129, 130]: therefore, the dominant processes limiting capacity attainment and retention are attributable to features of the cathode matrix under development. This enables evaluation of the pore size distribution, surface area, and other

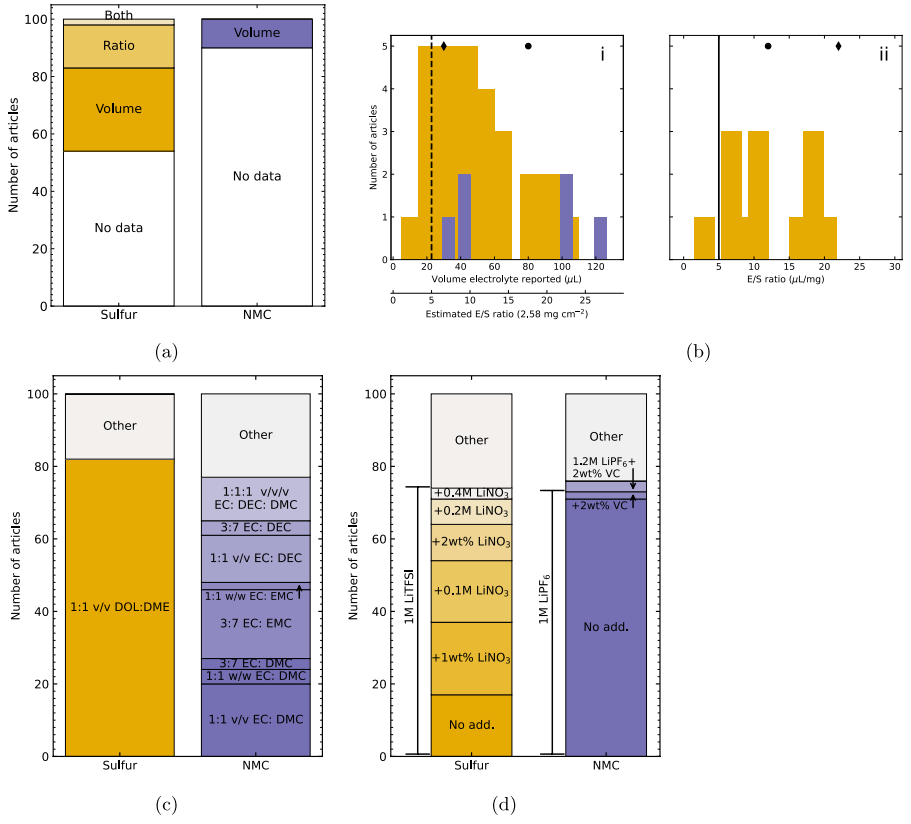

Fig. 6 Frequency of reporting electrolyte-related parameters. **a** Electrolyte content by volume (μL) or ratio (μL mg^{-2} active material). **b** Volume of electrolyte (i) and E/S ratio (ii). Offset *x* axis in (i) shows estimated E/S ratio for average sulfur areal loading and 15 mm diameter electrode; markers show two reports where both volume and ratio are reported. Vertical line indicates 5μ L E/S ratio target from Ref [49]. **c** Electrolyte solvent combinations. DOL: 1, 3-dioxolane, DME: 1, 2 dimethoxyethane, EC: ethylene carbonate, DEC: diethyl carbonate, DMC: dimethyl carbonate, EMC: ethyl methyl carbonate. v/v: volume ratio, w/w: weight ratio. **d** Salt and electrolyte additive combinations. LiTFSI: Lithium bis(trifluoromethanesulfonyl)imide, VC: vinyl carbonate, No add.: No additive.'Other' includes all electrolyte solvent combinations with 1 report

parameters without the electrolyte limiting reversible sulfur utilisation. By contrast, the electrolyte accounts for a smaller proportion of the mass of practical NMC-based cells (∼10 % [131], 1.3 g Ah^{-1} [132] approximately equivalent to 4.7:1 electrolyte: NMC by mass) due to the higher mass density of the NMC cathode and graphite anode than their counterparts in Li–S cells. The electrolyte content was most commonly reported as the absolute volume per coin cell, rather than as an E/S ratio, which is attributable to the practical accessibility of this value, however the offset x-axis of Fig. 6b shows an estimated corresponding E/S ratio based on the mean sulfur areal loading (2.58 mg cm^{-2}) and coin cell electrode diameter of 1.5 cm. The skew towards lower E/S ratios in Fig. 6b, combined with the increased frequency of E/S ratio and/ or electrolyte volume reporting in Li–S cells after c. 2019 (Fig. 10a) suggests that authors are more likely to report instances of proactively aiming to minimise the E/S ratio, while omitting the quantity used in cells with excess electrolyte.

Figure 6 compares the frequency with which different electrolyte solvents (a) and salt/ electrolyte additive combinations (b) are used in the articles included in this meta-analysis. As shown in Fig. 6c, 81 Li–S articles use 1:1 v/v 1,2-dimethoxyethane: 1,3-dioxolane (referred to as DOL:DME) as the electrolyte solvent, while Li-ion cells with NMC cathodes use a more diverse range of solvent combinations. DOL: DME is an established electrolyte solvent for Li–S batteries with conventional liquid electrolytes due to the solubility for LiPS provided by DME [133], and the role of DOL in forming an ionically conducting, electronically insulating layer on the lithium metal anode to prevent ongoing electrolyte decomposition [43, 109, 134]. In Li-ion cells with NMC cathodes, the cyclic molecule ethylene carbonate (EC) is commonly used in conjunction with linear carbonates including dimethyl carbonate (DMC), diethyl carbonate (DEC), or ethyl methyl carbonate (EMC). EC has a high dielectric constant and is consequently conducive to $LiPF_6$ dissociation, and forms an effective SEI on graphite anodes [135, 136]. However, EC has a melting point of 36.4 °C, so is solid at room temperature conditions [135, 136]. To form a liquid electrolyte with sufficiently low viscosity to wet the porous electrodes, linear carbonates are used as co-solvents, including in commercial electrolytes such as LP30 (1:1 v/v EC: DMC with 1 M $LiPF_6$) [137] and LP57 (3:7 EC/EMC with 1 M $LiPF_6$) [138], corresponding to the most frequently used solvent combinations shown in Fig. 6c.

By contrast, as shown in Fig. 6d the use of electrolyte salt and additives is more consistent in the Li-ion samples reviewed in this meta-analysis, with 75 articles using 1 M $LiPF_6$ salt without additives, while Li–S samples consistently use 1 M LiTFSI electrolyte salt with a greater variety of $LiNO_3$ concentrations. $LiNO_3$ is used to promote the growth of a continuous passivating film on the lithium anode to prevent ongoing reactions between the anode and dissolved polysulfides in the electrolyte, thereby mitigating the LiPS shuttle effect [134, 139]. Additionally, $LiNO_3$ catalyses the oxidation of long-chain LiPS to S_8, lowering the required driving force for the reaction and thereby protecting the integrity of pathways in the electrically conducting host matrix [140]. However, due to gas evolution by $LiNO_3$ at $\leq$40 °C [141], $LiNO_3$ is not compatible with UN Recommendations on the Transport of Dangerous Goods [48], meaning that effective elimination of $LiNO_3$ from Li–S electrolyte is necessary for widespread adoption of Li–S batteries.

5.6 Cyclic voltammetry

Although the application of a constant current in galvanostatic cyclic is more representative of discharging a battery through a load, complementary information can be obtained from cyclic voltammetry (CV). Galvanostatic cycling and CV are therefore inequivalent physical processes, however comparing the total duration of CV sweeps with galvanostatic C rate indicates whether conclusions about reaction kinetics are derived from tests which are representative of target galvanostatic operating conditions. Figure 7 compares the duration of CV sweeps (crosses) with C rates (ranges terminated by dots) in articles included in this meta-analysis. In 32% and 11% of Li–S and NMC articles respectively, a single CV rate was reported which fell within the same range of durations as the galvanostatic cycling rates. Figure 7 also shows that CV is more widely used in Li–S research than NMC. By contrast, dQ/dV analysis is widely employed in NMC research but was only found in 1 Li–S article [142]. In the Li-ion intercalation system, dQ/dV analysis highlights phase transitions and degradation processes associated with the sloping voltage profile [143]. However in the Li–S system, the two-plateau discharge curve can be intuitively interpreted for information about the overpotential and relative capacity derived from each step of the reaction.

The use of multiple CV sweep rates can also be used to infer the Li^+ diffusion coefficient, and the range of sweep rates over which the electrochemical behaviour is mass transport rather than rate limited, where a higher diffusion coefficient over a wider operating window is indicative of cells with higher cycling rate capability. Among the articles included in this meta-analysis, the Randles-Ševčik equation relating CV sweep rate (v) to diffusion coefficient was reported by 1 Li–S [144] and 1 NMC [145] article. While both confirmed that the peak current value (i_p) increased linearly with $v^{1/2}$, 1 condition on the validity of the Randles-Ševčik equation and recommended in the JPS voluntary reporting guidelines [5], in both cases the peak overpotential increased with increasing $v^{1/2}$ thereby limiting the equation's strict applicability. Further examples of multiple CV sweep rate use were to confirm the reversibility of Li–S conversion reactions [146], and to differentiate between Faradaic and non-Faradaic electron transfer processes in NMC [147]. Alternative methods of inferring the diffusion coefficient of novel electrode materials seen in this meta-analysis included galvanostatic intermittent titration (GITT), all

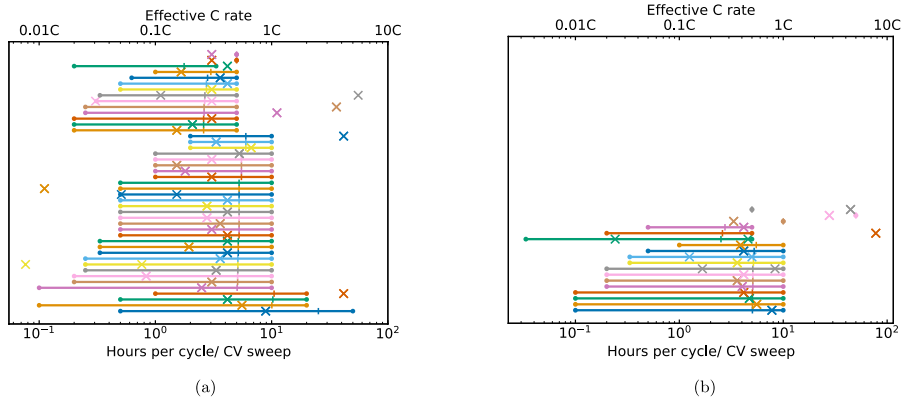

Fig. 7 Comparison of range of C rates (spans, with linear midpoint indicated by vertical marker) and equivalent duration of CV sweep in hours (crosses) reported in the same article: one span per article where both CV and galvanostatic cycling are reported for **a** Li–S and **b** NMC electrodes

in NMC articles [98, 148, 149], and electrochemical impedance spectroscopy (EIS, see Sect. 5.7), used for this purpose in 3 NMC articles [62, 150, 151].

5.7 Electrochemical impedance spectroscopy

EIS can be used to infer the number of electron transfer processes in an electrochemical system, grouped by their resistive and reactive response at different perturbation frequencies. As a non-destructive process, it can be applied to cells undergoing conventional galvanostatic cycling to investigate changes in the presence and relative contribution of different interfaces to electron transfer processes, subject to cells being allowed to equilibrate before measurement. Equivalent circuit models (ECMs) can provide an intuitive representation of electron transfer processes, although their interpretation is ambiguous as multiple ECM configurations can be used to fit the same data. The non-unique attribution of ECMs to EIS spectra is reflected by the variation in the number of ECM elements reported by articles included in this meta-analysis, shown in Fig. 5b. Here, the number of 'elements' refers to the number of ECM components in series. Here, an 'element' may therefore refer to a resistor modelling the Ohmic resistance of the electrolyte, a Warburg element, or Voigt circuit with a resistor and constant phase element in parallel with each other: despite the differences between these 'elements', this is used here as a bases for comparison because each series 'element' typically represents a modelled interface or electron transfer process. In NMC articles, 18 use 4 element ECMs, typically comprising an Ohmic resistor, two Voigt elements, and a Warburg element to represent electrolyte resistance, SEI and charge transfer impedance, and bulk diffusion respectively (e.g. [123, 147, 152]). Li–S articles use ECMs with an Ohmic resistor, typically with 2 Voigt elements to represent the passivation layer at the lithium anode and charge-transfer resistance between the electrolyte and LiPS (e.g. [117, 153, 154]), although the representation of bulk diffusion varies, with some articles using Voigt or constant phase elements (CPE) (e.g. [155]) and others using Warburg elements (e.g. [60, 117]). In semi-quantitative usage, ECMs provide comparisons of the relative contributions of interfacial processes to cell impedance, for example by tracking the change of impedance contributions with similar characteristic frequencies (and therefore likely similar physical interpretation) throughout a time series of EIS spectra for the same cell [155]. Similarly, 2 articles in this meta-analysis illustrated the change in physical phenomena contributing to cell impedance before and after cycling using ECMs fitted to EIS spectra acquired before and after cell cycling [70, 125], incorporating an additional Voigt element to represent charge transfer impedance after an initial formation cycle (see Sect. 5.3).

The variation in ECM fitting between articles is partly attributable to the aforementioned ambiguity in interpretation: where distinct physical processes contributing to the impedance have similar characteristic frequency, they may be indistinguishable from each other in the Argand plane. Although not applied in any of the articles included in this meta-analysis, since c. 2017 in Li-ion [156] and c. 2022 in Li–S, distribution of relaxation times analysis has been increasingly applied to differentiate features in the time domain which overlap in the frequency domain while reducing reliance on the analyst's judgement about the number of features to fit. For example, Ref [156] identified distinct contributions from the current collector and SEI from a broad, overlapping peak in Li-ion anodes, while Ref [157] identified up to 8 distinct contributions to Li–S

impedance, including up to 4 from the overlapping broad semi-circle at low-mid frequencies. While ECM fitting tools are frequently embedded in potentiostat software, open-source DRT analysis tools such as the DRTtools MATLAB add-on [158] are available. In addition to ambiguity of interpretation, a further reason variation between the ECM models selected by different articles is indicated by Ref [159], where EIS spectra for multiple cells from the same batch are compared, showing qualitatively different spectra throughout their cycling life, including different relative contributions from impedance contributions attributed to different physical processes. However, consistent attribution of impedance contributions elucidated by DRT showed that the contribution from SEI was dominant in predicting capacity fade and cell failure in Li–S cells with lithium metal anodes. Analysis of the trends in impedance contributions, particularly those strongly correlated with cell degradation, may therefore yield more transferable information than direct comparison of EIS spectra or discrete fitting values due to the variability between cells with nominally identical parameters. However, the variability in models fitted to derive these parameters highlights the challenges with direct comparison of quantitative impedance values reported in different articles.

6 Physical characterisation

6.1 Measurand distribution

In Fig. 8, all of the measurands are shown on the same y-axis to highlight the prevalence of characterising the raw materials and occasional reporting of *post-mortem* electrodes. This is attributable to the challenges with requiring specialised cells for *in-situ*,

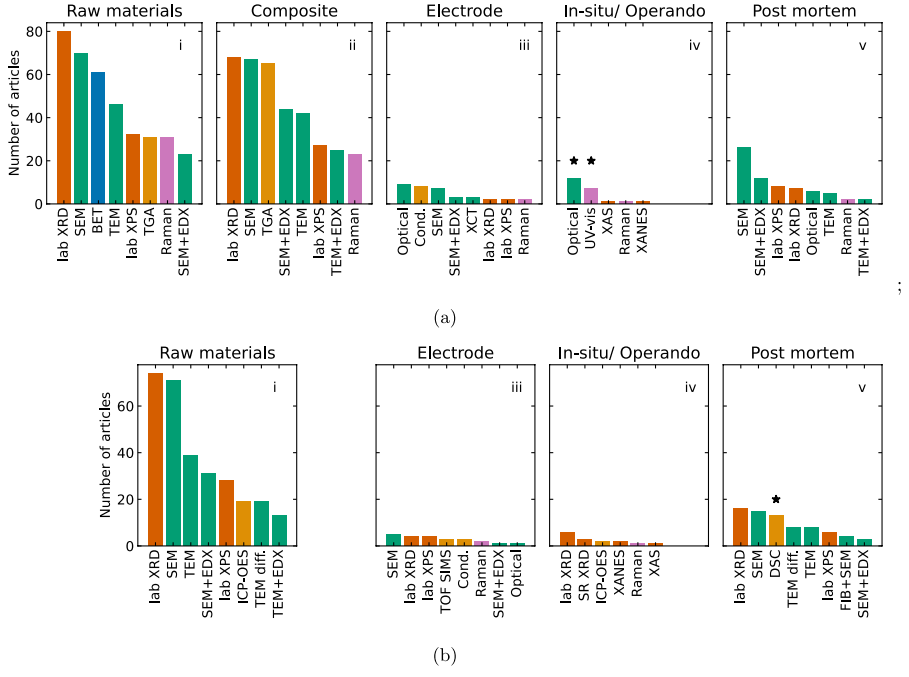

Fig. 8 Summary of most frequently applied techniques to different measurands for Li–S (**a**) and NMC (**b**) related articles, showing the 8 most commonly used for each measurand. Raw materials: for Li–S, refers to host matrix separate from active sulfur; for NMC, refers to NMC powder. Composite: for Li–S, refers to sulfur/ host composite (not applicable to NMC, bii intentionally omitted). Electrode: uncycled electrode including binder, additive, and current collector. *In-situ/ operando*: cell with electrolyte undergoing electrochemical testing, or electrolyte and electrode undergoing chemical reaction (see text). *Post-mortem*: electrode removed from cell after electrochemical cycling, characterised without electrolyte or anode

with geometry different from standard coin cells, and experimental compatibility with time-resolved measurement [160, 161]: synchrotron X-ray diffraction (XRD), X-ray absorption spectroscopy (XAS), and X-ray absorption near edge spectroscopy (XANES) are among the techniques reported for *in-situ* characterisation in this meta-analysis (Fig. 8a iv and 8b iii). For Li–S, optical photographs and UV–vis in Fig. 8b iv and marked with an asterisk were categorised as *'in-situ'*, but correspond to photographs comparing the colour change of LiPS solutions [86, 117, 142, 146, 162–167], or UV–vis spectra of LiPS solutions [73, 164, 166, 168–170] following adsorption of LiPS species onto host matrices to demonstrate their efficacy in preventing inventory loss by diffusion. Similarly, differential scanning calorimetry (DSC) is marked with an asterisk and shown as *post-mortem* as it is typically applied after lithiation of the NMC and deconstruction of the cell. By contrast, uncycled electrodes appear to be more accessible measurands than *in-situ* cells undergoing electrochemistry, however the focus of articles in this meta-analysis was CAM development, and therefore direct comparison of synthesis outputs is facilitated by characterising them in the absence of binder and low mass density, high volume fraction carbon black additives. Notably, where electrical conductivity is reported (13 % of Li–S articles, 9 % of NMC articles), it is most commonly reported for the uncycled electrode: this is rational because it includes the electrically conductive network incorporating conductive carbon additives. As previously noted [7], consistent reporting of the electrical conductivity of uncycled, as-synthesised electrodes does enable direct comparison between reports, but does not necessarily represent changes relevant to operating electrodes, such as binder swelling due to electrolyte interactions [171].

6.2 Evaluating active material synthesis

Figure 9 shows that the most frequently used characterisation techniques for both Li–S and NMC are SEM and XRD, providing complementary information about the $\sim$1 μm scale morphology and the $\sim$Å scale crystal structure. However, the different information requirements are shown by the application of techniques to different measurands in Fig. 8. The need to confirm the efficacy of S/C composite synthesis technique in producing an homogenous layer of sulfur at the host/ electrolyte interface is seen by comparing Fig. 8ai to Fig. 8bii: SEM with EDX (generally EDX mapping), is more frequently applied to the S/C composite than the raw materials to demonstrate the uniformity of sulfur distribution, while 66 of 80 Li–S articles reporting XRD for the raw materials also report it for the S/C composite. As previously discussed [7], this XRD comparison is frequently used to demonstrate whether the composite synthesis method results in bulk, crystalline α-S_8 or a thin, amorphous layer [44]. Similarly, as shown in 8ai and ii, Raman spectroscopy is used to compare the S/C composite with the raw materials in 22 articles: unlike the attenuation of XRD peaks associated with amorphous S_8 relative to α-S_8, the Raman spectrum depends only on the D_{4d} symmetry of S_8 molecules. When investigating carbon-based conductive host matrices, Raman spectroscopy is typically used to infer the effect of processing, including heating for the melt-infiltration of sulfur (e.g. [172–174]), *via* the I(D)/I(G) ratio, although decreasing I(D)/I(G) ratio is not uniquely correlated with increasing graphitic domain size [175].

Furthermore, 65 of Li–S articles report TGA for the S/C composite, with 30 reporting TGA for both the composite and 'raw materials'. Where it is reported for 'raw materials'

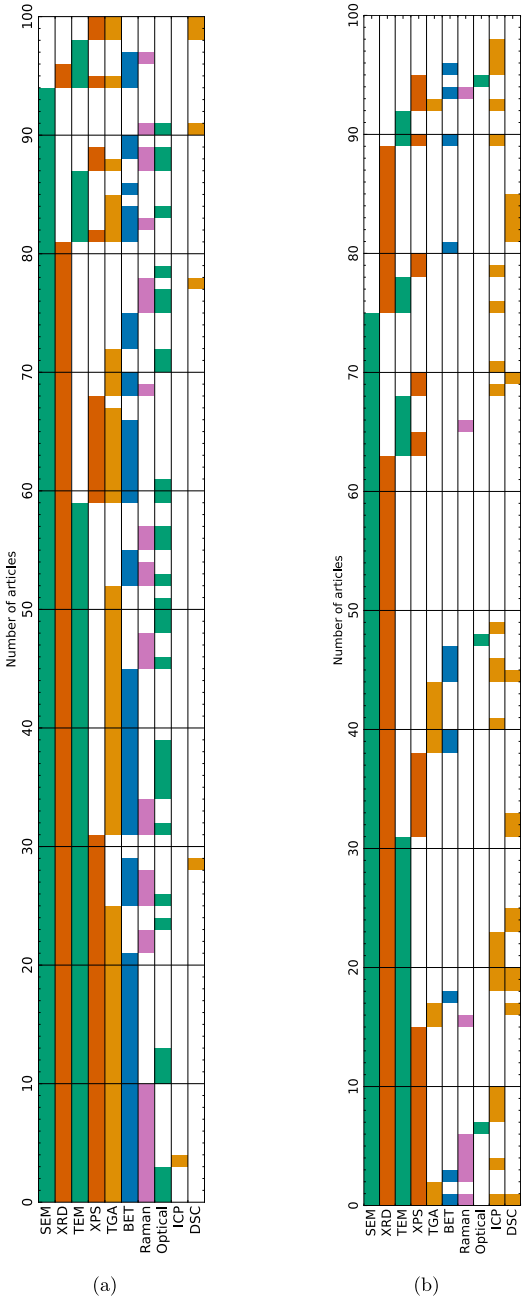

Fig. 9 Most frequently used combinations of characterisation techniques for **a** Li–S and **b** NMC related articles with a focus on the 10 most commonly reported techniques. Each row corresponds to one article, with colour blocks in corresponding columns indicating techniques used in each article. Combinations are grouped with the most frequently used at the bottom. SEM: Scanning electron microscopy, XRD: X-ray diffraction, TEM: transmission electron microscopy, XPS: X-ray photoemission spectroscopy, TGA: Thermogravimetric analysis, BET: N_2 absorption surface area analysis, ICP: inductively coupled plasma, DSC: differential scanning calorimetry. SEM and TEM include imaging and energy dispersive X-ray (EDX) spectroscopy

in Fig. 8a, this is often to compare the mass loss profile of the S/C composite to sulfur to validate the temperature of mass loss, and/ or to compare the slightly delayed period of sulfur loss after incorporation into the S/C composite as evidence of encapsulation of the sulfur in the matrix (e.g. [44, 93, 153]). TGA is utilised to provide confirmation of S/C composite composition following melt infiltration, *in-situ* chemical formation by

reduction of $Na_2S_2O_3$ or Na_2S_x, or solution of sulfur in CS_2 or toluene: although the concentration or quantities of input reactants can be known, losses during synthesis are otherwise difficult to quantify. Since the metal oxide constituents of NMC electrodes are more refractory, inductively coupled plasma (ICP) is used more commonly in NMC-focussed articles to confirm the composition of raw materials, however a minority (9) NMC articles do report TGA with differential thermal analysis for example, to quantify the oxygen content [176] or to demonstrate mass loss corresponding to phase transitions [25] or calcination processes [177, 178]. Furthermore, given the small quantities typically used in these materials development-focussed articles (see Sect. 4.1), ~0.1 mg losses contribute significantly to measurement uncertainty, making analytical confirmation useful.

SEM and XRD are also the characterisation techniques most frequently applied to NMC, however by contrast to the binary presence/ absence indication of α-S_8 peaks in S/C composite XRD spectra, Rietveld refinement is routinely used in NMC-focussed articles to characterise its structural geometry, reflecting the need for reversible (de-) intercalation of Li^+ ions rather than the non-topotactic chemical conversion of sulfur. This is supported by the more frequent use of TEM with diffraction in NMC-related articles, and the use of *in-situ* XRD to monitor the structural distortion of the inter-layer *c*-spacing in layered oxides compared to the intra-layer *a*-spacing. During the first charge, the *c*-spacing initially increases due to repulsion between O^{2-} sites in the absence of Li^+, before decreasing towards the end of charge due to attraction between O^{2-} and transition metal ions (e.g. [27, 179–181]). Subsequent XRD spectra acquired for NMC electrodes, both in modified cell configurations for *in-situ* characterisation and extracted for *post-mortem* characterisation from conventional cells (Fig. 8biv, v) show that these structural changes remain stable after the first cycle (e.g. [27, 180, 182]).

6.3 Structural characterisation

XPS is reported by 46 % of Li–S and 32 % of NMC articles in this meta-analysis, although distinct information is sought for each battery chemistry and each measurand. In Li–S, examples of XPS use include probing the extent of host matrix/ active material interaction and the role of oxygen containing functional groups (e.g. [183, 184]), with Ref [57] using the surface sensitivity of XPS to demonstrate the role of binder distribution on host matrix/ active material interaction. Unlike other characterisation techniques including XRD and EDX, XPS differentiates between lithium-containing species including Li_2S_x ($x \geq 1$) formed during cycling, and $Li_2S_xO_y$-containing compounds indicative of irreversible reaction products between the sulfur and electrolyte. In *post-mortem* samples extracted from cycled Li–S cells, XPS has therefore been used to identify deposits responsible for pore-blocking (e.g. [60]) and to verify the efficacy of functional groups and dopants in anchoring LiPS (e.g. [185, 186]). An analogous application of XPS in *post-mortem* NMC electrodes (and their corresponding anodes) is the characterisation of the CEI and SEI, where analysis of differentiated carbon- and oxygen-containing group peaks provides insights into the contribution of decomposed carbonate electrolyte solvents and $LiPF_6$ salt. This has been used to infer the role of electrochemical cycling conditions (e.g. [187]) and the influence of cathode interface morphology and composition (e.g. [99]) on SEI/ CEI composition, which in turn affects the interfacial impedance and electrolyte degradation processes in the cell. In addition to interfacial interactions, in

NMC electrodes, XPS is applied to identify the valence states of Ni, Mn, and Co (e.g. [51, 188]) and in some instances to quantify the proportion of surface species in each valence state, for example the relative content of Ni^{2+} vs. Ni^{3+} [189, 190].

6.4 Pore size distribution and surface area

The different energy storage mechanisms in Li–S and NMC require different priorities in quantitative physical characterisation techniques, including pore size distribution of the carbon host matrix in Li–S, and (less frequently) particle size distribution in NMC. The specific surface area (SSA) and pore size distribution are typically determined using N_2 adsorption isotherms, with the SSA determined using the multipoint BET (Brunauer-Emmett-Teller) equation, although 2 Li–S [74, 94] and 1 NMC [191] articles report mercury intrusion porosimetry. In Li–S, the SSA and particle size distribution are most commonly measured for the carbon host matrix (Fig. 8a), with 20 articles contrasting this with measurements for the composite to demonstrate the degree of pore filling by the sulfur (e.g. [44, 153, 192]). However, since the volatility of sulfur means that the degassing process of heating under vacuum to remove adsorbed water cannot be used prior to measurement, values for composites are likely to represent underestimates [44]. In addition to the initial sulfur particle size [118, 193], the pore size distribution and SSA of Li–S electrodes is correlated with the amount of electrolyte required to wet the surface [49] (see Sect. 5), whereas the particle size distribution of NMC dictates the diffusion distance of Li^+ ions to intercalant at the centre of the article, and possible cracking-based degradation mechanisms [194]. Consequently, 6 NMC articles report laser-diffraction or dynamic light scattering particle size determination methods [79, 87, 97, 176, 195, 196], (plus 2 Li–S articles [94, 168]). Meanwhile, 5 NMC articles [2, 36, 79, 152, 197] and 6 Li–S articles [71, 84, 166, 198–200] report particle size distributions determined SEM micrographs, e.g. statistics from 50 measured particles. In Li–S, the most commonly used method of calculating pore size distribution is the BJH (Barrett-Joyner-Halenda) equation (23 articles), which may underestimate the pore size for pores less than 10 nm [201], however two articles [77, 125] specified both the BJH and HK (Horvath and Kawazoe) which enables the determination of micropores $\leq$2 nm [201, 202]. While density functional theory (DFT)-based methods are compatible with micropore determination [201], adoption and specification of consistent a pore size determination method such as the most widely-reported BJH would enable correlation of electrochemical behaviour with quantifiable trends in SSA and pore size distribution, despite systematic limitations in the micropore range.

7 Discussion

In quantifying the frequency with which different synthesis and testing parameters are reported for NMC and Li–S, despite the higher TRL of NMC electrodes, it is clear that there is still space for standardisation in the suite of reported parameters for both chemistries. Given the motivation of direct comparison between articles, this is likely to be a self-fulfilling trend. The frequency of reporting selected parameters with time is represented in heat maps in Fig. 10, showing an overall trend of increased frequency and completeness of parameter reporting with time. The 100 articles for each battery chemistry currently included in this meta-analysis represent a small fraction of the total available, hence the heat maps in Fig. 10 are indicative of a sample rather than quantifying

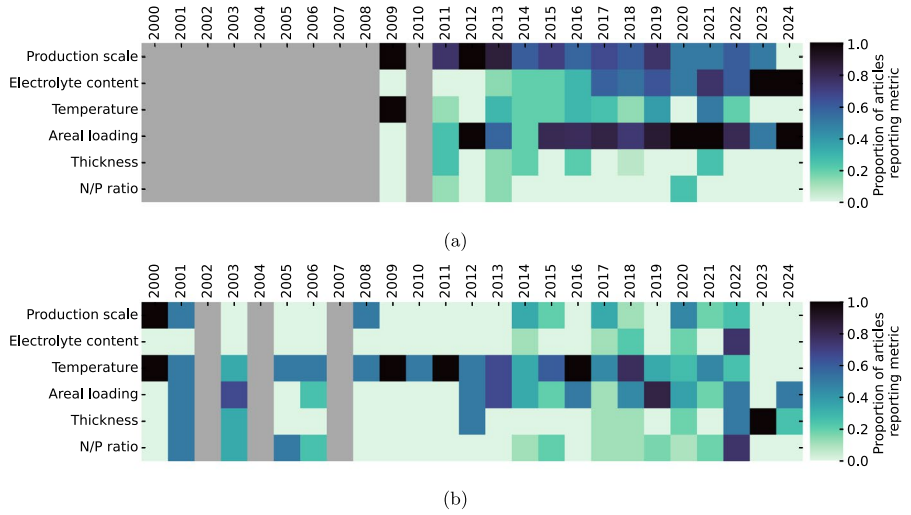

Fig. 10 Proportion of articles for each year included in the meta-analysis reporting the listed metrics. (Grey indicates no articles available in that year within the meta-analysis). Some years contain data from single articles, and the figure represents only data from within the dataset of 200 articles

an overall trend, however the data collated for this work is intended as a foundation for a larger database. The parameters shown in these heat maps were selected for their ease of measurement, as a subset of recommended parameters from the voluntary reporting guidelines (recommended parameters that are currently universally reported, for example wt% mass of binder, cell format, and electrolyte composition are omitted from these time series). In principle, the production scale and electrolyte volume do not require any additional measurement, but their reporting would lead to more reproducible research. In a benchmarking study, Ref [203] compared solid-state cells made with identical constituents but using different assembly protocols in different labs, including different orders of assembly and different assembly environments, with the obtained results showing wide variation, demonstrating how the standardisation of routine protocols which are not directly associated with the materials development affect the reproducibility of the conclusions drawn. Similarly, Ref [204] demonstrated the effect of "trivial" parameters in cell assembly on Li–S cells specifically, including the pressure used during cell crimping and auxiliary component thickness, with marked differences in stable capacity and early cell failure. Many of the factors investigated by Ref [204] are included in journal voluntary reporting checklists, specifically in checklist [5], however of the 200 articles included in this meta analysis only 1 [197] included a battery-specific voluntary reporting checklist in its supplementary information, with a further article [100] including a reproducibility checklist that is non-specific to battery research. Despite the availability of the voluntary reporting checklists, correspondence with 3 of the 5 journals indicates that their implementation is not currently routinely tracked. Notably, the single example where a checklist is included does not report every suggested metric: even more frequent reporting of incomplete checklists would identify common blind spots, and may prompt the standardisation of commonly-used parameters even where they remain non-optimised.

Naturally, in these articles selected for their focus on cathode materials development, non-optimised parameters associated with auxiliary cell components which would not be directly compatible with scale-up to commercial cells, may go unreported because

they appear to detract from the competitiveness of the material [205]. Approximately 20 stoichiometries of NMC-related materials other than established/ integer compositions were included in this meta-analysis, ranging from high Ni (e.g. $LiNi_{0.96}Mn_{0.01}Co_{0.03}O_2$ [206]) to high Mn (e.g. $LiNi_{0.13}Mn_{0.54}Co_{0.13}O_2$ [190]). Meanwhile, Li–S host matrix morphologies ranged from 'starfish-like' [207] to 'French fries-like' [163], and the materials explored ranged from bio-derived soybean hulls [174] and waste tea [208] to highly ordered covalent organic frameworks [209]. It is unrealistic to require all reports of novel materials to demonstrate their feasibility directly in lean electrolyte, low N/P, prototype cells following scalable synthesis procedures when such studies typically work with half-cells using ~100 mg of the candidate material (see Sect. 4). However, using electrolyte/ active ratio as an example, it is likely that excess electrolyte is being used in all such exploratory cells, and it may be possible to identify materials-specific advancements among novel materials tested in conservative, but comparable conditions where the volume of electrolyte is consistently reported.

Beyond the frequently reported parameters and established characterisation techniques discussed in Sects. 5 and 6, there are opportunities for extracting additional useful information from routine measurements. More frequent reporting of the parameters included in Fig. 10 would both aid reproducibility and enable investigation of correlations between these parameters and cell performance. A further example related to Li–S galvanostatic cycling data is the ratio between the capacity attained at each discharge plateau, and the respective polarisation of each plateau, which is often described qualitatively. However, 6 articles quantified these values and identified trends throughout the cycling life of cells, enabling identification of materials with higher sulfur utilisation and lower polarisation [58, 74, 93, 144, 163, 163].

The database collated during this work catalogues values and references for key parameters, and is available in the Supplementary Information: there is scope for expansion beyond the extant 200 articles. In addition to cross-referencing within the database to identify trends, the database can also serve as a directory for identifying input parameters for numerical modelling. For example, where no single article contains all of the required parameters, filtering the database by cell chemistry, electrode composition, and cell configuration (i.e. half cell/ full cell) can be used to find mutually compatible sets of parameters.

8 Conclusions

This meta-analysis collated data on the electrode synthesis, electrochemical testing, and physical characterisation reported for 100 Li–S and 100 NMC-focussed research articles published between 2000 and 2024 to identify trends in data reporting with the progression of TRL. Among the parameters with relevance to both battery chemistries, there is variability in whether the values are reported for each electrode type, and where they are present, there is further variability in the methods of applications and data analysis protocols.

Comparing the reporting frequencies for the technologies reveals opportunities for more complete reporting without additional experimental work in future articles. Although the ultimate aim of materials-level research is the scale-up and commercialisation of improved battery technology, this leads to the omission of fundamental parameters from research publications as they do not appear optimised for commercial

viability. However, reporting such values, even where non-optimised, would enable direct comparison of electrochemical results from different studies, and improve reproducibility as each inter-dependent cell component is optimised. Li–S articles are more likely than NMC to report the areal loading of active material (73% for Li–S vs. 37% for NMC), which can be determined using the average mass of electrodes of known geometric area. This is indicative of the electrode thickness, which is required for reproducibility, but is infrequently measured directly (11% Li–S and 12% NMC). Similarly, Li–S articles are more likely to report the scale of synthesis (64% for Li–S vs. 21% for NMC), which is also likely to impact reproducibility *via* its effects on slurry mixing homogeneity and and the availability of suitable equipment to enable scaled-up synthesis within the required parameter tolerances. For other parameters, simple additional measurements and records could contribute to enhanced reproducibility, including the temperature of cells during cycling, which is presently reported more frequently in NMC (45%) than Li–S (23%). Although controlled, constant temperature cycling provides the most directly comparable results, the sensitivity of cell performance to temperature means that reporting the minimum, maximum, and average temperature experienced by cells in 'room temperature' laboratories is instructive when comparing results between articles.

Despite the focus on cathode development in this meta-analysis, the complex interaction between cell components means that the reporting of electrochemical results from cells with novel cathode chemistry in combination with non-standard electrolytes and non-standard voltage ranges makes it difficult to identify correlations between individual parameters and cell performance, as demonstrated for Li–S cells in Ref [7]. Although more widespread use of reporting checklists such as Refs [2–6] will aid improvements in reproducibility, this meta-analysis does not identify 'beach head' parameters to prioritise for reporting in future articles as key determinants of reproducibility. Of the 200 articles surveyed, only 1 reported electrochemical data averaged from multiple cells [101], otherwise it is assumed that each article reports data from a single cell for each parameter combination. However, known from the experience of experimentalists in the battery development field, and documented quantitively in Refs [159, 203], cells produced using materials from the same batch and assembled using nominally similar procedures may have different initial capacities, rates of capacity decay, and failure mechanisms. Therefore, more frequent reporting of the electrochemical data from repeat samples in future articles would provide an immediate insight into the sensitivity of cell performance to auxiliary parameters and aid identification of priority parameters for standardisation.

The data collation and analysis framework established in a previous report [7] and expanded here provides a flexible basis for comparing other trends in the battery literature. Having evaluated materials-level trends and variability in Li–S coin cells, there is scope for expanding this methodology to pilot-line and laboratory-scale cell development.

Supplementary Information

The online version contains supplementary material available at https://doi.org/10.1007/s44373-026-00099-1.

Supplementary file 1 (pdf 146 KB)

Supplementary file 2 (csv 282 KB)

Acknowledgements
The authors are grateful to Dr. Till von Graberg (Advanced Energy Materials, Wiley), Dr. Yohan Dall'Agnese, (Joule, Cell), and Ashley Hicks (ACS Energy Letters) for correspondence about the active implementation and tracking the usage of voluntary reporting guidelines.

Author contributions
L. R. B. developed the Python code for the graphical user interface, entered the data, performed the analysis, and prepared the manuscript. Y. S. and B. P. checked the code functionality, contributed to data entry, and reviewed the manuscript. J. B. R. and P. R. S. were responsible for supervision, project and resources administration, funding acquisition, editing and reviewing of the manuscript.

Funding
The authors would like to acknowledge the Faraday Institution (Faraday.ac.uk; EP/S003053/1) for funding the energy storage work at the Advanced Propulsion Lab, UCL, and Department of Engineering Sciences, University of Oxford, in particular through the LiSTAR programme (FIRG083). J.B.R. would like to acknowledge Innovate UK for financial support (Project Number: 10040939). P.R.S. also acknowledged the Royal Academy of Engineering Chair in Emerging Technologies (CiET1718\59) and the Department of Science, Innovation and Technology (DSIT).

Data availability
All data aggregated and analysed for this publication are available as a.csv file in the Supplementary Information. The code developed for the graphical user interface is available at the following URL: https://github.com/LiamBird/meta-characterisation.git.

Declarations

Ethics approval and consent to participate
Not applicable.

Consent for publication
Not applicable.

Competing interests
The authors declare no competing interests.

Received: 20 October 2025 / Accepted: 17 January 2026
Published online: 10 April 2026

References

1. Ellerington I. Faraday Report 2020. High-Energy Battery Technologies (Faraday Institution, 2020).
2. Sun Y-K. An experimental checklist for reporting battery performances. ACS Energy Lett. 2021;6:2187–9.
3. Margherita M, Aurora A, Quartaone E. Batteries Europe Guidelines on common reporting methodology, Batteries Europe, 2025.
4. Stephan AK. Standardized Battery Reporting Guidelines Joule. 2021;5:1–2.
5. Li J, Arbizzani C, Kjelstrup S, Xiao J, Xia Y-Y, Yu Y, et al. Good practice guide for papers on batteries for the Journal of Power Sources. J Power Sources. 2020;452:227824.
6. Wiley VCH battery reporting checklist.
7. Bird LR, Robinson JB, Shearing PR. Progress in carbon cathodic host matrices for lithium–sulfur cells: a meta analysis. ACS Mater Lett. 2024;6:5363–74.
8. Yari S, Conde Reis A, Pang Q, Safari M. Performance benchmarking and analysis of lithium–sulfur batteries for next-generation cell design. Nat Commun. 2025;16:5473.
9. Kilic A, Odabaş Ç, Yildirim R, Eroglu D. Assessment of critical materials and cell design factors for high performance lithium–sulfur batteries using machine learning. Chem Eng J. 2020;390:124117.
10. Robinson JB, Xi K, Kumar RV, Ferrari AC, Au H, Titirici M-M, et al. 2021 roadmap on lithium sulfur batteries. J Phys Energy. 2021;3:031501.
11. Gifford S. Lithium, Cobalt and Nickel: The Gold Rush of the 21st Century, 6 (The Faraday Institution, 2022).
12. ESTO. Definition Of Technology Readiness Levels, NASA, 2005.
13. Dörfler S, Althues H, Härtel P, Abendroth T, Schumm B, Kaskel S. Challenges and key parameters of lithium–sulfur batteries on pouch cell level. Joule. 2020;4:539–54.
14. International Energy Agency (IEA). Global EV Outlook 2023 (2023).
15. Li M, Lu J, Chen Z, Amine K. 30 years of lithium-ion batteries. Adv Mater. 2018;30:1800561.
16. Bin Abu Sofian ADA, Imaduddin IS, Majid S, Kurniawan TA, Chew KW, Lay C-H, Show PL. Nickel-rich nickel-cobalt-manganese and nickel-cobalt-aluminum cathodes in lithium-ion batteries: pathways for performance optimization. J Clean Prod. 2024;435:140324.
17. Chen S, Zhang X, Xia M, Wei K, Zhang L, Zhang X, et al. Issues and challenges of layered lithium nickel cobalt manganese oxides for lithium-ion batteries. J Electroanal Chem. 2021;895:115412.
18. Saaid FI, Kasim MF, Winie T, Elong KA, Azahidi A, Basri ND, et al. Ni-rich lithium nickel manganese cobalt oxide cathode materials: a review on the synthesis methods and their electrochemical performances. Heliyon. 2024;10:e23968.
19. Mizushima K, Jones P, Wiseman P, Goodenough J. LixCoO2 (0). Mater Res Bull. 1980;15:783–9.
20. Paulsen JM, Thomas CL, Dahn JR. O2 structure Li2/3 Ni1/3 Mn2/3 O2: a new layered cathode material for rechargeable lithium batteries. I. Electrochem Prop J Electrochem Soc. 2000;147:861.

21. Thackeray MM, De Kock A, Rossouw MH, Liles D, Bittihn R, Hoge D. Spinel electrodes from the Li–Mn–O system for rechargeable lithium battery applications. J Electrochem Soc. 1992;139:363–6.
22. Lu Z, MacNeil DD, Dahn JR. Layered Li[Ni[sub x]Co[sub 1–2x]Mn[sub x]]O[sub 2] cathode materials for lithium-ion batteries. Electrochem Solid-State Lett. 2001;4:A200.
23. Liu Z, Yu A, Lee JY. Synthesis and characterization of LiNi1xyCoxMnyO2 as the cathode materials of secondary lithium batteries. J Power Sources. 1999;81–82:416–9.
24. Belharouak I, Sun Y-K, Liu J, Amine K. Li(Ni1/3Co1/3Mn1/3)O2 as a suitable cathode for high power applications. J Power Sources. 2003;123:247–52.
25. Noh H-J, Youn S, Yoon CS, Sun Y-K. Comparison of the structural and electrochemical properties of layered Li[NixCoyMnz]O2 (x = 1/3, 0.5, 0.6, 0.7, 0.8 and 0.85) cathode material for lithium-ion batteries. J Power Sources. 2013;233:121–30.
26. Li J, Wang L, Zhang Q, He X. Synthesis and characterization of LiNi0.6Mn0.4xCoxO2 as cathode materials for Li-ion batteries. J Power Sources. 2009;189:28–33.
27. Li Z, Zhang J, Lou XW. Hollow carbon nanofibers filled with MnO_2 nanosheets as efficient sulfur hosts for lithium–sulfur batteries. Angew Chem Int Ed. 2015;54:12886–90.
28. Kim M-H, Shin H-S, Shin D, Sun Y-K. Synthesis and electrochemical properties of Li[Ni0.8Co0.1Mn0.1]O2 and Li[Ni0.8Co0.2]O2 via co-precipitation. J Power Sources. 2006;159:1328–33.
29. Wang B, Gim J, Son S-B, Shkrob IA, Abraham DP, Trask SE, et al. Electrolyte study for high-nickel $LiNi_{0.9}Mn_{0.05}Co_{0.05}O_2$ cathodes. J Electrochem Soc. 2023;170:020505.
30. Banza Lubaba Nkulu C, Casas L, Haufroid V, De Putter T, Saenen ND, Kayembe-Kitenge T, Musa Obadia P, Kyanika Wa Mukoma D, Lunda Ilunga J-M, Nawrot TS, Luboya Numbi O, Smolders E, Nemery B. Sustainability of artisanal mining of cobalt in DR Congo. Nat Sustain. 2018;1:495–504.
31. Harlow JE, Ma X, Li J, Logan E, Liu Y, Zhang N, et al. A wide range of testing results on an excellent lithium-ion cell chemistry to be used as benchmarks for new battery technologies. J Electrochem Soc. 2019;166:A3031-44.
32. Gomez-Martin A, Reissig F, Frankenstein L, Heidbüchel M, Winter M, Placke T, et al. Magnesium substitution in Ni-rich NMC layered cathodes for high-energy lithium ion batteries. Adv Energy Mater. 2022;12:2103045.
33. Sallard S, Sheptyakov D, Villevieille C. Improved electrochemical performances of Li-rich nickel cobalt manganese oxide by partial substitution of Li + by Mg 2+. J Power Sources. 2017;359:27–36.
34. Sattar T, Lee S-H, Sim S-J, Jin B-S, Kim H-S. Effect of Mg-doping on the electrochemical performance of LiNi0.84Co0.11Mn0.05O2 cathode for lithium ion batteries. Int J Hydrogen Energy. 2020;45:19567–76.
35. Zhou F, Zhao X, Lu Z, Jiang J, Dahn J. The effect of Al substitution on the reactivity of delithiated LiNi1/3Mn1/3Co(1/3-z)AlzO2 with non-aqueous electrolyte. Electrochem Commun. 2008;10:1168–71.
36. Samarasingha PB, Wijayasinghe A, Behm M, Dissanayake L, Lindbergh G. Development of cathode materials for lithium ion rechargeable batteries based on the system Li(Ni1/3Mn1/3Co(1/3-x)Mx)O2, (M=Mg, Fe, Al and x=0.00 to 0.33). Solid State Ionics. 2014;268:226–30.
37. Breuer O, Chakraborty A, Liu J, Kravchuk T, Burstein L, Grinblat J, et al. Understanding the role of minor molybdenum doping in $LiNi_{0.5}Co_{0.2}Mn_{0.3}O_2$ electrodes: from structural and surface analyses and theoretical modeling to practical electrochemical cells. ACS Appl Mater Interfaces. 2018;10:29608–21.
38. Theion. Theions's Crystal Battery. Theion, 2025.
39. Energy Z. Zeta Energy: Leading the charge. Zeta Energy;2025.
40. Gelion. Gelion: The Sufur Battery Company, Gelion, 2025.
41. Lyten. Lyten: Lithium–sulfur batteries Lyten, 2025.
42. Yamin H, Peled E. Electrochemistry of a nonaqueous lithium/sulfur cell. J Power Sources. 1983;9:281–7.
43. Peled E, Sternberg Y, Gorenshtein A, Lavi Y. Lithium–sulfur battery: evaluation of dioxolane-based electrolytes. J Electrochem Soc. 1989;136:1621–5.
44. Ji X, Lee KT, Nazar LF. A highly ordered nanostructured carbon–sulphur cathode for lithium–sulphur batteries. Nat Mater. 2009;8:500–6.
45. Li X, Li X, Banis MN, Wang B, Lushington A, Cui X, et al. Tailoring interactions of carbon and sulfur in Li–S battery cathodes: significant effects of carbon-heteroatom bonds. J Mater Chem A. 2014;2:12866.
46. Hou T-Z, Chen X, Peng H-J, Huang J-Q, Li B-Q, Zhang Q, et al. Design principles for heteroatom-doped nanocarbon to achieve strong anchoring of polysulfides for lithium–sulfur batteries. Small. 2016;12:3283–91.
47. Zhang SS. Heteroatom-doped carbons: synthesis, chemistry and application in lithium/sulphur batteries. Inorg Chem Front. 2015;2:1059–69.
48. United Nations. Recommendations on the transport of dangerous goods—manual of tests and criteria. New York: United Nations; 2015.
49. Bhargav A, He J, Gupta A, Manthiram A. Lithium–sulfur batteries: attaining the critical metrics. Joule. 2020;4:285–91.
50. Shao Y, Pang B, Bird L, Robinson JB, Shearing PR. Contemporary trends in lithium–sulfur battery design: a comparative review of liquid, quasi-solid, and all-solid-state architectures and mechanisms. Adv Energy Mater 2025;e03239.
51. Xi X, Fan Y, Liu Y, Chen Z, Zou J, Zhu S. Enhanced cyclic stability of NCM-622 cathode by Ti3+ doped TiO2 coating. J Alloy Compd. 2021;872:159664.
52. Yan P, Zheng J, Zhang J-G, Wang C. Atomic resolution structural and chemical imaging revealing the sequential migration of Ni Co, and Mn upon the battery cycling of layered cathode. Nano Lett. 2017;17:3946–51.
53. Jung H-C, Han D, Kim D-W, Ahn B. Synthesis of the nickel–cobalt-manganese cathode material using recycled nickel as precursors from secondary batteries. Arch. Metall. Mater. 2021;987–990.
54. Dreger H, Bockholt H, Haselrieder W, Kwade A. Discontinuous and continuous processing of low-solvent battery slurries for lithium nickel cobalt manganese oxide electrodes. J Electr Mater. 2015;44:4434–43.
55. Liang X, Rangom Y, Kwok CY, Pang Q, Nazar LF. Interwoven MXene nanosheet/carbon-nanotube composites as Li–S cathode hosts. Adv Mater. 2017;29:1603040.
56. Ouyang L, Wu Z, Wang J, Qi X, Li Q, Wang J, et al. The effect of solid content on the rheological properties and microstructures of a Li-ion battery cathode slurry. RSC Adv. 2020;10:19360–70.
57. Shaibani M, Mirshekarloo MS, Singh R, Easton CD, Cooray MCD, Eshraghi N, Abendroth T, Dörfler S, Althues H, Kaskel S, Hollenkamp AF, Hill MR, Majumder M. Expansion-tolerant architectures for stable cycling of ultrahigh-loading sulfur cathodes in lithium-sulfur batteries. Sci. Adv. 2020;6:eaay2757.

58. Yari S, Bird L, Rahimisheikh S, Reis AC, Mohammad M, Hadermann J, et al. Probing charge transport and microstructural attributes in solvent- versus water-based electrodes with a spotlight on Li–S battery cathode. Adv Energy Mater. 2024;14:2402163.
59. Tancin RJ, ÖzdoÄŸru B, Dutta NS, Finegan DP, Tremolet De Villers BJ. Direct reuse of graphite and lithium nickel manganese cobalt oxide (NMC) recovered from ultrafast-laser ablation debris in Li-ion battery electrodes. J Power Sources. 2024;596:234027.
60. Huang Z, Shi T, Cheng J, Liao Y, Ji H, Huang Y, et al. Balancing sulfur utilization and electrolyte demand in Li–S batteries via porosity-tuned calendaring-driven electrodes. J Power Sources. 2025;643:237052.
61. Wang H-Y, Mei S-L, Tan X-L, Lu B-H, Li N, Wang Z-B. Unveiling the particle-feature influence of lithium nickel manganese cobalt oxide on the high-rate performances of practical lithium-ion batteries. J Alloy Compd. 2025;1010:177774.
62. Jia X, Yan M, Zhou Z, Chen X, Yao C, Li D, et al. Nd-doped LiNi0.5Co0.2Mn0.3O2 as a cathode material for better rate capability in high voltage cycling of Li-ion batteries. Electrochim Acta. 2017;254:50–8.
63. Chen Y, Zhang Y, Chen B, Wang Z, Lu C. An approach to application for LiNi0.6Co0.2Mn0.2O2 cathode material at high cutoff voltage by TiO2 coating. J Power Sources. 2014;256:20–7.
64. Pettinger K-H, Dong W. When does the operation of a battery become environmentally positive? J Electrochem Soc. 2017;164:A6274-7.
65. Thomitzek M, Von Drachenfels N, Cerdas F, Herrmann C, Thiede S. Simulation-based assessment of the energy demand in battery cell manufacturing. Procedia CIRP. 2019;80:126–31.
66. Bresser D, Buchholz D, Moretti A, Varzi A, Passerini S. Alternative binders for sustainable electrochemical energy storage—the transition to aqueous electrode processing and bio-derived polymers. Energy Environ Sci. 2018;11:3096–127.
67. Savvidou EK, Rensmo A, Benskin JP, Schellenberger S, Hu X, Weil M, et al. PFAS-free energy storage: investigating alternatives for lithium-ion batteries. Environ Sci Technol. 2024;58:21908–17.
68. Walker BA, Plaza-Rivera CO, Sun S-S, Lu W, Connell JW, Lin Y. Dry-pressed lithium nickel cobalt manganese oxide (NCM) cathodes enabled by holey graphene host. Electrochim Acta. 2020;362:137129.
69. Li J, Qiu W, Liu X, Zhang Y, Zhao Y. NiCo-layered double hydroxide to composite with sulfur as cathodes for high-performance lithium–sulfur batteries. ChemElectroChem. 2022;9:e202101211.
70. Yan Y, Shi M, Zou Y, Wei Y, Chen L, Fan C, et al. Tunable hierarchical porous carbon aerogel/graphene composites cathode matrix for Li–S batteries. J Alloy Compd. 2019;791:952–61.
71. Li G, Sun J, Hou W, Jiang S, Huang Y, Geng J. Three-dimensional porous carbon composites containing high sulfur nanoparticle content for high-performance lithium-sulfur batteries. Nat Commun. 2016;7:10601.
72. Duan L, Zhao L, Cong H, Zhang X, Lü W, Xue C. Plasma treatment for nitrogen-doped 3D graphene framework by a conductive matrix with sulfur for high-performance Li–S batteries. Small. 2019;15:1804347.
73. Zhong L, Yang K, Guan R, Wang L, Wang S, Han D, et al. Toward theoretically cycling-stable lithium–sulfur battery using a foldable and compositionally heterogeneous cathode. ACS Appl Mater Interfaces. 2017;9:43640–7.
74. Gueon D, Hwang JT, Yang SB, Cho E, Sohn K, Yang D-K, et al. Spherical macroporous carbon nanotube particles with ultrahigh sulfur loading for lithium–sulfur battery cathodes. ACS Nano. 2018;12:226–33.
75. Zhu J, Pitcheri R, Kang T, Guo Y, Li J, Qiu Y. Electrospun carbon nanofibers decorated with MnO nanoparticles as a sulfur-absorbent for lithium–sulfur batteries. Ceram Int. 2018;44:16837–43.
76. Zhou G, Li L, Ma C, Wang S, Shi Y, Koratkar N, et al. A graphene foam electrode with high sulfur loading for flexible and high energy Li–S batteries. Nano Energy. 2015;11:356–65.
77. Ganesan A, Varzi A, Passerini S, Shaijumon MM. Graphene derived carbon confined sulfur cathodes for lithium–sulfur batteries: electrochemical impedance studies. Electrochim Acta. 2016;214:129–38.
78. Jung R, Morasch R, Karayaylali P, Phillips K, Maglia F, Stinner C, et al. Effect of ambient storage on the degradation of Ni-rich positive electrode materials (NMC811) for Li-Ion batteries. J Electrochem Soc. 2018;165:A132-41.
79. Zehetmaier PM, Zoller F, Beetz M, Plaß MA, Häringer S, Böller B, et al. Nanocellulose-mediated transition of lithium-rich pseudo-quaternary metal oxide nanoparticles into lithium nickel cobalt manganese oxide (NCM) nanostructures. ChemNanoMat. 2020;6:618–28.
80. Hendrickx M, Paulus A, Kirsanova MA, Van Bael MK, Abakumov AM, Hardy A, et al. The influence of synthesis method on the local structure and electrochemical properties of Li-Rich/Mn-Rich NMC cathode materials for Li-Ion batteries. Nanomaterials. 2022;12:2269.
81. Song SH, Cho M, Park I, Yoo J-G, Ko K-T, Hong J, et al. High-voltage-driven surface structuring and electrochemical stabilization of Ni-rich layered cathode materials for Li rechargeable batteries. Adv Energy Mater. 2020;10:2000521.
82. Xi K, Kidambi PR, Chen R, Gao C, Peng X, Ducati C, et al. Binder free three-dimensional sulphur/few-layer graphene foam cathode with enhanced high-rate capability for rechargeable lithium sulphur batteries. Nanoscale. 2014;6:5746–53.
83. Liu L-J, Chen Y, Zhang Z-F, You X-L, Walle MD, Li Y-J, et al. Electrochemical reaction of sulfur cathodes with Ni foam current collector in Li–S batteries. J Power Sources. 2016;325:301–5.
84. Seh ZW, Li W, Cha JJ, Zheng G, Yang Y, McDowell MT, et al. Sulphur-TiO2 yolk-shell nanoarchitecture with internal void space for long-cycle lithium–sulphur batteries. Nat Commun. 2013;4:1331.
85. Tao Z, Yang Z, Guo Y, Zeng Y, Xiao J. Plane double-layer structure of AC@S cathode improves electrochemical performance for lithium–sulfur battery. Front. Chem. 2018;6.
86. Zhang J, Hu H, Li Z, Lou XW. Double-shelled nanocages with cobalt hydroxide inner shell and layered double hydroxides outer shell as high-efficiency polysulfide mediator for lithium–sulfur batteries. Angew Chem Int Ed 2016;55.
87. Shiozaki M, Yamashita H, Hirayama Y, Ogami T, Kanamura K. Blending lithium nickel manganese cobalt oxide with lithium iron manganese phosphate as cathode materials for lithium-ion batteries with enhanced electrochemical performance. Electrochemistry. 2023;91:077007–077007.
88. Lv D, Zheng J, Li Q, Xie X, Ferrara S, Nie Z, et al. High energy density lithium-sulfur batteries: challenges of thick sulfur cathodes. Adv Energy Mater. 2015;5:1402290.
89. Singh M, Kaiser J, Hahn H. Thick electrodes for high energy lithium ion batteries. J Electrochem Soc. 2015;162:A1196-201.
90. Chen H, Zhou G, Boyle D, Wan J, Wang H, Lin D, et al. Electrode design with integration of high tortuosity and sulfur-philicity for high-performance lithium–sulfur battery. Matter. 2020;2:1605–20.
91. Cooper S, Bertei A, Shearing P, Kilner J, Brandon N. TauFactor: an open-source application for calculating tortuosity factors from tomographic data. SoftwareX. 2016;5:203–10.

92. Liu J, Ding Y, Shen Z, Zhang H, Han T, Guan Y, et al. A lamellar yolk–shell lithium–sulfur battery cathode displaying ultralong cycling life, high rate performance, and temperature tolerance. Adv Sci. 2022;9:2103517.
93. Fang R, Li G, Zhao S, Yin L, Du K, Hou P, et al. Single-wall carbon nanotube network enabled ultrahigh sulfur-content electrodes for high-performance lithium–sulfur batteries. Nano Energy. 2017;42:205–14.
94. Moschner R, Gerle M, Danner T, Simanjuntak EK, Michalowski P, Latz A, et al. Impact of the sulfurized polyacrylonitrile cathode microstructure on the electrochemical performance of lithium–sulfur batteries. Adv Sci. 2025;12:2415436.
95. Uzun K, Alolaywi H, Thapa S, Frieberg B, Wang M, Huang X, et al. Investigating the effect of electrode compositions on dry-made NMC811 positive electrodes. J Electrochem Soc. 2024;171:080532.
96. Sun H-H, Manthiram A. Impact of microcrack generation and surface degradation on a nickel-rich layered Li[$Ni_{0.9}Co_{0.05}Mn_{0.05}$]$O_2$ cathode for lithium-ion batteries. Chem Mater. 2017;29:8486–93.
97. Ren D, Padgett E, Yang Y, Shen L, Shen Y, Levin BDA, et al. Ultrahigh rate performance of a robust lithium nickel manganese cobalt oxide cathode with preferentially orientated li-diffusing channels. ACS Appl Mater Interfaces. 2019;11:41178–87.
98. Kim JW, Travis JJ, Hu E, Nam K-W, Kim SC, Kang CS, et al. Unexpected high power performance of atomic layer deposition coated Li[Ni1/3Mn1/3Co1/3]O2 cathodes. J Power Sources. 2014;254:190–7.
99. Fan X, Hu G, Zhang B, Ou X, Zhang J, Zhao W, et al. Crack-free single-crystalline Ni-rich layered NCM cathode enable superior cycling performance of lithium-ion batteries. Nano Energy. 2020;70:104450.
100. Sun HH, Kim U-H, Park J-H, Park S-W, Seo D-H, Heller A, et al. Transition metal-doped Ni-rich layered cathode materials for durable Li-ion batteries. Nat Commun. 2021;12:6552.
101. Neudeck S, Walther F, Bergfeldt T, Suchomski C, Rohnke M, Hartmann P, et al. Molecular surface modification of NCM622 cathode material using organophosphates for improved li-ion battery full-cells. ACS Appl Mater Interfaces. 2018;10:20487–98.
102. Primo EN, Chouchane M, Touzin M, Vazquez P, Franco AA. Understanding the calendering processability of Li(Ni0.33Mn0.33Co0.33)O2-based cathodes. J Power Sources. 2021;488:229361.
103. US Advanced Battery Consortium. Goals for Advanced High-Performance Batteries for Electric Vehicle (EV) Applications.
104. Yang X-G, Liu T, Ge S, Rountree E, Wang C-Y. Challenges and key requirements of batteries for electric vertical takeoff and landing aircraft. Joule. 2021;5:1644–59.
105. Reid HT, Singh G, Palin E, Dai Y, Zong W, Somerville L, et al. Key considerations for cell selection in electric vertical take off and landing vehicles: a perspective. EES Batteries. 2025;1:227–41.
106. EUROBAT TF Innovation. White paper Batteries Innovation Roadmap 2035. (Association of European Automotive and Industrial Battery Manufacturers, 2024).
107. Hettesheimer T, Neef C, Rosellón Inclán I, Link S, Schmaltz T, Schuckert F, Stephan A, Stephan M, Thielmann A, Weymann L, Wicke T. :unav. Lithium-Ion Battery Roadmap - Industrialization Perspectives toward 2030 (Fraunhofer-Gesellschaft, 2023).
108. Zhang SS. Role of LiNO3 in rechargeable lithium/sulfur battery. Electrochim Acta. 2012;70:344–8.
109. Zhang SS. Liquid electrolyte lithium/sulfur battery: fundamental chemistry, problems, and solutions. J Power Sources. 2013;231:153–62.
110. Páez Fajardo GJ, Fiamegkou E, Gott JA, Wang H, Temprano I, Seymour ID, et al. Synergistic degradation mechanism in single crystal Ni-rich NMC//graphite cells. ACS Energy Lett. 2023;8:5025–31.
111. McNulty RC, Hampson E, Cutler LN, Grey CP, Dose WM, Johnson LR. Understanding the limits of Li-NMC811 half-cells. J Mater Chem A. 2023;11:18302–12.
112. Mao Y, Wang X, Xia S, Zhang K, Wei C, Bak S, et al. High-voltage charging-induced strain, heterogeneity, and micro-cracks in secondary particles of a nickel-rich layered cathode material. Adv Funct Mater. 2019;29:1900247.
113. Ryu H-H, Park K-J, Yoon CS, Sun Y-K. Capacity fading of Ni-rich Li[Ni_x Co_y Mn_{1-x-y}]O_2 (0.6 *x* 0.95) cathodes for high-energy-density lithium-ion batteries: Bulk or surface degradation? Chem Mater 30, 2018;1155–1163.
114. Dose WM, Morzy JK, Mahadevegowda A, Ducati C, Grey CP, De Volder MFL. The influence of electrochemical cycling protocols on capacity loss in nickel-rich lithium-ion batteries. J Mater Chem A. 2021;9:23582–96.
115. Gan L, Chen R, Yang X, Xu X, Zan M, Li Q, et al. Comparative study on high-voltage safety performance of LiNixMnyCozO2 cathode with different nickel contents. Appl Phys Lett. 2022;121:203901.
116. Zheng H, Sun Q, Liu G, Song X, Battaglia VS. Correlation between dissolution behavior and electrochemical cycling performance for LiNi1/3Co1/3Mn1/3O2-based cells. J Power Sources. 2012;207:134–40.
117. Li T, Bo H, Cao H, Lai Y, Liu Y, Huang Z. Effects of carbon hosts on electrochemical properties of lithium–sulfur batteries. Int J Electrochem Sci. 2017;12:5731–41.
118. Di Lecce D, Marangon V, Du W, Brett DJ, Shearing PR, Hassoun J. The role of synthesis pathway on the microstructural characteristics of sulfur–carbon composites: X-ray imaging and electrochemistry in lithium battery. J Power Sources. 2020;472:228424.
119. Krätzig O, Degen F. A comprehensive review and analysis of technology performance characteristics of lithium-ion battery cell manufacturing: introducing a call-for-innovation-heatmap. J Power Sources Adv. 2025;33:100174.
120. Degen F, Winter M, Bendig D, Tübke J. Energy consumption of current and future production of lithium-ion and post lithium-ion battery cells. Nat Energy. 2023;8:1284–95.
121. Feinauer M, Wohlfahrt-Mehrens M, Hölzle M, Waldmann T. Temperature-driven path dependence in Li-ion battery cyclic aging. J Power Sources. 2024;594:233948.
122. Liang L, Du K, Peng Z, Cao Y, Duan J, Jiang J, et al. Co-precipitation synthesis of Ni0.6Co0.2Mn0.2(OH)2 precursor and characterization of LiNi0.6Co0.2Mn0.2O2 cathode material for secondary lithium batteries. Electrochim Acta. 2014;130:82–9.
123. Zhang M, Hu G, Wu L, Peng Z, Du K, Cao Y. A facile approach to enhance high-cutoff voltage cycle stability of LiNi0.5Co0.2Mn0.3O2 cathode materials using lithium titanium oxide. Electrochim Acta. 2017;232:80–8.
124. Johnson CS, Li N, Lefief C, Vaughey JT, Thackeray MM. Synthesis, characterization and electrochemistry of lithium battery electrodes: x Li_2 MnO_3. (1–x)$LiMn_{0.333}$ $Ni_{0.333}$ $Co_{0.333}$ O_2 (0 x 0.7). Chem Mater 2008;20:6095–106.
125. Wu F, Zhao S, Chen L, Lu Y, Su Y, Li J, et al. Electron bridging structure glued yolk-shell hierarchical porous carbon/sulfur composite for high performance Li–S batteries. Electrochim Acta. 2018;292:199–207.
126. Zhou Z, Li G, Zhang J, Zhao Y. Wide working temperature range rechargeable lithium-sulfur batteries: a critical review. Adv Funct Mater. 2021;31:2107136.
127. Zhang H, Chen J, Li Z, Peng Y, Xu J, Wang Y. Operating lithium–sulfur batteries in an ultrawide temperature range from -50 °C to 70 °C. Adv Funct Mater. 2023;33:2304433.

128. Andrei P, Shen C, Zheng JP. Theoretical and experimental analysis of precipitation and solubility effects in lithium–sulfur batteries. Electrochim Acta. 2018;284:469–84.
129. Fan FY, Chiang Y-M. Electrodeposition kinetics in Li–S batteries: effects of low electrolyte/sulfur ratios and deposition surface composition. J Electrochem Soc. 2017;164:A917-22.
130. Liu Y, Elias Y, Meng J, Aurbach D, Zou R, Xia D, et al. Electrolyte solutions design for lithium–sulfur batteries. Joule. 2021;5:2323–64.
131. Hagen M, Hanselmann D, Ahlbrecht K, Maça R, Gerber D, Tübke J. Lithium–sulfur cells: the gap between the state-of-the-art and the requirements for high energy battery cells. Adv Energy Mater. 2015;5:1401986.
132. Chen S, Niu C, Lee H, Li Q, Yu L, Xu W, et al. Critical parameters for evaluating coin cells and pouch cells of rechargeable Li-metal batteries. Joule. 2019;3:1094–105.
133. Rajput NN, Murugesan V, Shin Y, Han KS, Lau KC, Chen J, et al. Elucidating the solvation structure and dynamics of lithium polysulfides resulting from competitive salt and solvent interactions. Chem Mater. 2017;29:3375–9.
134. Aurbach D, Pollak E, Elazari R, Salitra G, Kelley CS, Affinito J. On the surface chemical aspects of very high energy density. Rechargeable Li–sulfur batteries. J Electrochem Soc. 2009;156:A694.
135. Xu K. Nonaqueous liquid electrolytes for lithium-based rechargeable batteries. Chem Rev. 2004;104:4303–418.
136. Xu K. Electrolytes and interphases in Li-ion batteries and beyond. Chem Rev. 2014;114:11503–618.
137. Breddemann U, Banov K, Khodeir M, Novák P. Electrolytes for lithium-ion batteries: chemical changes over time and in the presence of impurities. ChemElectroChem. 2025;12:e202500017.
138. Lechtenfeld C-T, Buchmann J, Hagemeister J, Bela MM, Van Wickeren S, Stock S, et al. Analyzing the effect of electrolyte quantity on the aging of lithium-ion batteries. Adv Sci. 2024;11:2405897.
139. Tan J, Ye M, Shen J. Deciphering the role of $LiNO_3$ additives in Li–S batteries. Mater Horiz. 2022;9:2325–34.
140. Ye Y, Song M-K, Xu Y, Nie K, Liu Y-S, Feng J, et al. Lithium nitrate: a double-edged sword in the rechargeable lithium–sulfur cell. Energy Storage Mater. 2019;16:498–504.
141. Jozwiuk A, Berkes BB, Weiß T, Sommer H, Janek J, Brezesinski T. The critical role of lithium nitrate in the gas evolution of lithium–sulfur batteries. Energy Environ Sci. 2016;9:2603–8.
142. Hwa Y, Zhao J, Cairns EJ. Lithium sulfide (Li_2 S)/graphene oxide nanospheres with conformal carbon coating as a high-rate, long-life cathode for Li/S cells. Nano Lett. 2015;15:3479–86.
143. Honkura K, Honbo H, Koishikawa Y, Horiba T. State analysis of lithium-ion batteries using discharge curves. ECS Trans. 2008;13:61–73.
144. Kwon S, Song H, Çakmakçı N, Jeong Y. A practical approach to design sulfur host material for lithium–sulfur batteries based on electrical conductivity and pore structure. Mater Today Commun. 2021;27:102309.
145. Ma S, Hou X, Lin Z, Huang Y, Gao Y, Hu S, et al. One-pot facile co-precipitation synthesis of the layered Li1 + x (Mn0.6Ni0.2Co0.2)1–x O2 as cathode materials with outstanding performance for lithium-ion batteries. J Solid State Electrochem. 2016;20:95–103.
146. Dang M, Liu M, Li F. Mesoporous 3D titanium dioxide embed carbon nanofibers with superior polysulfide adsorption ability for high electrochemical performance Li–S batteries. Ionics. 2021;27:1531–6.
147. Chu C, Chang L, Yin D, Zhang D, Cheng Y, Wang L. Large-sized nickel–cobalt–manganese composite oxide agglomerate anode material for long-life-span lithium-ion batteries. ACS Appl Energy Mater. 2021;4:13811–8.
148. Kim H, Kim S-B, Park D-H, Park K-W. Fluorine-doped LiNi0.8Mn0.1Co0.1O2 cathode for high-performance lithium-ion batteries. Energies. 2020;13:4808.
149. Huang W, Lin C, Zhang M, Li S, Chen Z, Zhao W, et al. Revealing roles of Co and Ni in Mn-rich layered cathodes. Adv Energy Mater. 2021;11:2102646.
150. Xi Y, Liu Y, Zhang D, Jin S, Zhang R, Jin M. Comparative study of the electrochemical performance of LiNi0.5Co0.2Mn0.3O2 and LiNi0.8Co0.1Mn0.1O2 cathode materials for lithium ion batteries. Solid State Ion. 2018;327:27–31.
151. Zhang X, Mauger A, Lu Q, Groult H, Perrigaud L, Gendron F, et al. Synthesis and characterization of LiNi1/3Mn1/3Co1/3O2 by wet-chemical method. Electrochim Acta. 2010;55:6440–9.
152. Zhang Y, Wang Z, Zhong Y, Wu H, Li S, Cheng Q, et al. Coating for improving electrochemical performance of NCM523 cathode for lithium-ion batteries. Ionics. 2021;27:13–20.
153. Li H, Sun L, Zhao Y, Tan T, Zhang Y. Blackberry-like hollow graphene spheres synthesized by spray drying for high-performance lithium–sulfur batteries. Electrochim Acta. 2019;295:822–8.
154. Zhang J, Zhang Q, Qu X, Xu G, Fan B, Yan Z, et al. Hierarchically pyridinic-nitrogen enriched porous carbon for advanced sodium-ion and lithium–sulfur batteries: electrochemical performance and in situ Raman spectroscopy investigations. Appl Surf Sci. 2022;574:151559.
155. Waluś S, Barchasz C, Bouchet R, Alloin F. Electrochemical impedance spectroscopy study of lithium–sulfur batteries: useful technique to reveal the Li/S electrochemical mechanism. Electrochim Acta. 2020;359:136944.
156. Steinhauer M, Risse S, Wagner N, Friedrich KA. Investigation of the solid electrolyte interphase formation at graphite anodes in lithium-ion batteries with electrochemical impedance spectroscopy. Electrochim Acta. 2017;228:652–8.
157. Soni R, Robinson JB, Shearing PR, Brett DJ, Rettie AJ, Miller TS. Lithium–sulfur battery diagnostics through distribution of relaxation times analysis. Energy Storage Mater. 2022;51:97–107.
158. Wan TH, Saccoccio M, Chen C, Ciucci F. Influence of the discretization methods on the distribution of relaxation times deconvolution: implementing radial basis functions with DRTtools. Electrochim Acta. 2015;184:483–99.
159. Soni R, Hu J, Robinson JB, Rettie AJ, Miller TS. Predicting cell failure and performance decline in lithium–sulfur batteries using distribution of relaxation times analysis. Cell Rep Phys Sci. 2024;5:101833.
160. Santos ÉA, Amaral MM, Damasceno BS, Da Silva LM, Zanin HG, Weker JN, et al. Advanced in situ/operando characterizations of lithium-sulfur batteries: a sine qua non. Nano Energy. 2024;130:110098.
161. Llewellyn AV, Matruglio A, Brett DJL, Jervis R, Shearing PR. Using in-situ laboratory and synchrotron-based X-ray diffraction for lithium-ion batteries characterization: a review on recent developments. Condensed Matter. 2020;5:75.
162. Peng H-J, Zhang G, Chen X, Zhang Z-W, Xu W-T, Huang J-Q, et al. Enhanced electrochemical kinetics on conductive polar mediators for lithium–sulfur batteries. Angew Chem Int Ed. 2016;55:12990–5.
163. Yang X, Yan N, Zhou W, Zhang H, Li X, Zhang H. Sulfur embedded in one-dimensional French fries-like hierarchical porous carbon derived from a metal–organic framework for high performance lithium–sulfur batteries. J Mater Chem A. 2015;3:15314–23.

164. Lee E, Blauwkamp J, Castro FC, Wu J, Dravid VP, Yan P, et al. Exploring lithium–cobalt–nickel oxide spinel electrodes for 3.5 V Li-ion cells. ACS Appl Mater Interfaces. 2016;8:27720–9.
165. Li Z, Xu R, Deng S, Su X, Wu W, Liu S, et al. MnS decorated N/S codoped 3D graphene which used as cathode of the lithium–sulfur battery. Appl Surf Sci. 2018;433:10–5.
166. Xiao P, Bu F, Yang G, Zhang Y, Xu Y. Integration of graphene, nano sulfur, and conducting polymer into compact, flexible lithium–sulfur battery cathodes with ultrahigh volumetric capacity and superior cycling stability for foldable devices. Adv Mater. 2017;29:1703324.
167. Bao W, Xie X, Xu J, Guo X, Song J, Wu W, et al. Confined sulfur in 3 D MXene/reduced graphene oxide hybrid nanosheets for lithium–sulfur battery. Chem A Eur J. 2017;23:12613–9.
168. Song J, Gordin ML, Xu T, Chen S, Yu Z, Sohn H, et al. Strong lithium polysulfide chemisorption on electroactive sites of nitrogen-doped carbon composites for high-performance lithium–sulfur battery cathodes. Angew Chem Int Ed. 2015;54:4325–9.
169. Ousmane IA, Li R, Wang C, Li GR, Cai WL, Liu BH, et al. Fabrication of oriented-macroporous-carbon incorporated with -Al2O3 for high performance lithium–sulfur battery. Microporous Mesoporous Mater. 2018;266:276–82.
170. Zhu H, Li Q, Gong X, Cao K, Chen Z. Enhanced high voltage performance of chlorine/bromine co-doped lithium nickel manganese cobalt oxide. Curr Comput-Aided Drug Des. 2018;8:425.
171. Lacey MJ, Jeschull F, Edström K, Brandell D. Porosity blocking in highly porous carbon black by PVdF binder and its implications for the Li–S system. J Phys Chem C. 2014;118:25890–8.
172. Gómez-Urbano J, Gómez-Cámer J, Botas C, Díez N, López Del Amo J, Rodríguez-Martinez L, et al. Hydrothermally reduced graphene oxide for the effective wrapping of sulfur particles showing long term stability as electrodes for Li–S batteries. Carbon. 2018;139:226–33.
173. He Z, Dou X, Liu W, Zhang L, Lv L, Liu J, et al. Yeast-derived sulfur host for the application of sustainable Li–S battery cathode. Batteries. 2023;9:289.
174. Zhu Y, Xu G, Zhang X, Wang S, Li C, Wang G. Hierarchical porous carbon derived from soybean hulls as a cathode matrix for lithium–sulfur batteries. J Alloy Compd. 2017;695:2246–52.
175. Ferrari AC, Robertson J. Interpretation of Raman spectra of disordered and amorphous carbon. Phys Rev B. 2000;61:14095–107.
176. Fröhlich K, Legotin E, Bärhold F, Trifonova A. New large-scale production route for synthesis of lithium nickel manganese cobalt oxide. J Solid State Electrochem. 2017;21:3403–10.
177. Solmaz R, Karahan BD, Keles O. Fabrication of nickel manganese cobalt oxide (NMCO) anodes for lithium-ion batteries via hydrothermal process. J Appl Electrochem. 2020;50:1079–89.
178. Kanthachan J, Khamman O, Intatha U, Eitssayeam S. Effect of reducing calcination processing on structural and electrochemical properties of LiNi0.5Mn0.3Co0.2O2 cathode materials for lithium battery. Mater Today Proc 2021;47:3600–3.
179. El Aouam A, Sabi N, Aziam H, Touag O, Dolotko O, Mansori M, et al. Development and understanding of the lithiation/de-lithiation mechanism of a low cobalt and nickel-rich cathode material for lithium-ion batteries. J Power Sources. 2024;606:234551.
180. Weigel T, Schipper F, Erickson EM, Susai FA, Markovsky B, Aurbach D. Structural and electrochemical aspects of $LiNi_{0.8}Co_{0.1}Mn_{0.1}O_2$ cathode materials doped by various cations. ACS Energy Lett. 2019;4:508–16.
181. Li W, Asl HY, Xie Q, Manthiram A. Collapse of $LiNi_{1-x-y}Co_xMn_yO_2$ lattice at deep charge irrespective of nickel content in lithium-ion batteries. J Am Chem Soc. 2019;141:5097–101.
182. Li J, Huang J, Kong X, Zeng J, Zhao J. The apparent capacity decay by kinetic degradation of LiNi0.5Co0.2Mn0.3O2 during cycling under the high upper-limit charging potential. J Power Sources. 2021;496:229856.
183. Ji L, Rao M, Zheng H, Zhang L, Li Y, Duan W, et al. Graphene oxide as a sulfur immobilizer in high performance lithium/sulfur cells. J Am Chem Soc. 2011;133:18522–5.
184. Wang J, Liu Y, Cheng M, Zhao H, Wang J, Zhao Z, et al. Hierarchical porous carbon-graphene-based lithium–sulfur batteries. Electrochim Acta. 2019;318:161–8.
185. Peng Y, Li B, Wang Y, He X, Huang J, Zhao J. Prussian blue: a potential material to improve the electrochemical performance of lithium–sulfur batteries. ACS Appl Mater Interfaces. 2017;9:4397–403.
186. Du Z, Chen X, Hu W, Chuang C, Xie S, Hu A, et al. Cobalt in nitrogen-doped graphene as single-atom catalyst for high-sulfur content lithium–sulfur batteries. J Am Chem Soc. 2019;141:3977–85.
187. Wang H-Y, He X-F, Mei S-L, Zheng Y-P, Feng Y-W, Li N, et al. Boosting the cycling and storage performance of lithium nickel manganese cobalt oxide-based high-rate batteries through cathode manipulation. Electrochim Acta. 2024;474:143566.
188. Sun Y-K, Myung S-T, Park B-C, Prakash J, Belharouak I, Amine K. High-energy cathode material for long-life and safe lithium batteries. Nat Mater. 2009;8:320–4.
189. Fu C, Li G, Luo D, Li Q, Fan J, Li L. Nickel-rich layered microspheres cathodes: lithium/nickel disordering and electrochemical performance. ACS Appl Mater Interfaces. 2014;6:15822–31.
190. He B, Li A, Jin G, Wu H, Sun S, Liu D, et al. Li-rich Mn-based Li1.2Mn0.54 Ni0.13Co0.13O2 with carbothermal reduction coated spinel heterogeneous layer to enhance the electrochemical performance. Solid State Ionics. 2024;406:116457.
191. Huang Y, Wang Z-X, Li X-H, Guo H-J, Wang J-X. Synthesis of Ni0.8Co0.1Mn0.1(OH)2 precursor and electrochemical performance of LiNi0.8Co0.1Mn0.1O2 cathode material for lithium batteries. Trans Nonferrous Met Soc China. 2015;25:2253–9.
192. Zheng J, Tian J, Wu D, Gu M, Xu W, Wang C, et al. Lewis acid–base interactions between polysulfides and metal organic framework in lithium sulfur batteries. Nano Lett. 2014;14:2345–52.
193. Li X, Cao Y, Qi W, Saraf LV, Xiao J, Nie Z, et al. Optimization of mesoporous carbon structures for lithium–sulfur battery applications. J Mater Chem. 2011;21:16603.
194. Parks HCW, Boyce AM, Wade A, Heenan TMM, Tan C, Martínez-Pañeda E, et al. Direct observations of electrochemically induced intergranular cracking in polycrystalline NMC811 particles. J Mater Chem A. 2023;11:21322–32.
195. Liu W, Li X, Xiong D, Hao Y, Li J, Kou H, et al. Significantly improving cycling performance of cathodes in lithium ion batteries: The effect of Al2O3 and LiAlO2 coatings on LiNi0.6Co0.2Mn0.2O2. Nano Energy. 2018;44:111–20.
196. Zhang Y, Cao H, Zhang J, Xia B. Synthesis of LiNi0.6Co0.2Mn0.2O2 cathode material by a carbonate co-precipitation method and its electrochemical characterization. Solid State Ion. 2006;177:3303–7.
197. Viswanathan R, Pasupathi A, Subramaniam SEAVJY, Murugan R, Jose SP. Thermal plasma synthesis towards upscaling of multi-cation lithium nickel manganese cobalt oxide cathodes. J Power Sources. 2025;642:236943.

198. Du Z, Xu J, Jin S, Shi Y, Guo C, Kong X, et al. The correlation between carbon structures and electrochemical properties of sulfur/carbon composites for Li–S batteries. J Power Sources. 2017;341:139–46.
199. Shi Z, Yang Y, Huang Y, Yue H, Cao Z, Dong H, et al. Organic alkali metal salt derived three-dimensional N-doped porous carbon/carbon nanotubes composites with superior Li–S battery performance. ACS Sustain Chem Eng. 2019;7:3995–4003.
200. Zhang Y, Sun K, Liang Z, Wang Y, Ling L. N-doped yolk–shell hollow carbon sphere wrapped with graphene as sulfur host for high-performance lithium–sulfur batteries. Appl Surf Sci. 2018;427:823–9.
201. Thommes M, Cychosz KA. Physical adsorption characterization of nanoporous materials: progress and challenges. Adsorption. 2014;20:233–50.
202. Thommes M, Kaneko K, Neimark AV, Olivier JP, Rodriguez-Reinoso F, Rouquerol J, et al. Physisorption of gases, with special reference to the evaluation of surface area and pore size distribution (IUPAC Technical Report). Pure Appl Chem. 2015;87:1051–69.
203. Puls S, Nazmutdinova E, Kalyk F, Woolley HM, Thomsen JF, Cheng Z, et al. Benchmarking the reproducibility of all-solid-state battery cell performance. Nat Energy. 2024;9:1310–20.
204. Liao J, Ye Z. Nontrivial effects of trivial. Parameters on the performance of lithium–sulfur batteries. Batteries. 2018;4:22.
205. Johansson P, Alvi S, Ghorbanzade P, Karlsmo M, Loaiza L, Thangavel V, et al. Ten ways to fool the masses when presenting battery research. Batteries Supercaps. 2021;4:1785–8.
206. Tsai Y-T, Wu C-Y, Duh J-G. Synthesis of Ni-rich NMC cathode material by redox-assisted deposition method for lithium ion batteries. Electrochim Acta. 2021;381:138244.
207. Zhao S, Wei Z. Novel starfish-like M o_2C framework as efficient sulfur host for high electrochemical performance lithium–sulfur batteries. J Chem Tech Biotech. 2021;96:249–53.
208. Arie AA, Kristianto H, Cengiz EC, Demir-Cakan R. Waste tea-based porous carbon-sulfur composite cathodes for lithium–sulfur battery. Ionics. 2020;26:201–12.
209. Liao H, Ding H, Li B, Ai X, Wang C. Covalent-organic frameworks: potential host materials for sulfur impregnation in lithium–sulfur batteries. J Mater Chem A. 2014;2:8854–8.